Choi *et al. Energy Mater.* **2025**, *5*, 500062
DOI: 10.20517/energymater.2024.227

Energy Materials

Review

Open Access

Recent progress of photothermal catalysts for carbon dioxide conversion

Sang Hun Choi[1], Inhak Song[1,2,*], Wan Jae Dong[1,2,*]

[1]Department of Energy Environment Policy and Technology, Graduate School of Energy and Environment (KU-KIST Green School), Korea University, Seoul 02841, Republic of Korea.
[2]Department of Integrative Energy Engineering, College of Engineering, Korea University, Seoul 02841, Republic of Korea.

***Correspondence to:** Dr. Inhak Song, Department of Energy Environment Policy and Technology, Graduate School of Energy and Environment (KU-KIST Green School), Korea University, 145, Anam-ro, Seongbuk-gu, Seoul 02841, Republic of Korea; Department of Integrative Energy Engineering, College of Engineering, Korea University, 145, Anam-ro, Seongbuk-gu, Seoul 02841, Republic of Korea. E-mail: inhaksong@korea.ac.kr; Dr. Wan Jae Dong, Department of Energy Environment Policy and Technology, Graduate School of Energy and Environment (KU-KIST Green School), Korea University, 145, Anam-ro, Seongbuk-gu, Seoul 02841, Republic of Korea; Department of Integrative Energy Engineering, College of Engineering, Korea University, 145, Anam-ro, Seongbuk-gu, Seoul 02841, Republic of Korea. E-mail: wjdong@korea.ac.kr

How to cite this article: Choi, S. H.; Song, I.; Dong, W. J. Recent progress of photothermal catalysts for carbon dioxide conversion. *Energy Mater.* **2025**, *5*, 500062. https://dx.doi.org/10.20517/energymater.2024.227

Received: 28 Oct 2024 **First Decision:** 22 Nov 2024 **Revised:** 16 Dec 2024 **Accepted:** 26 Dec 2024 **Published:** 28 Feb 2025

Academic Editors: Ho Won Jang, Yuhui Chen **Copy Editor:** Fangling Lan **Production Editor:** Fangling Lan

Abstract

Photothermal catalysis has emerged as a promising strategy for converting carbon dioxide (CO_2) into value-added chemicals and fuels, offering a dual-energy approach that combines light and thermal energy to drive reactions under mild conditions. Photothermal effects are usually demonstrated by using plasmonic nanoparticles, which generate hot carriers and localized heating through light absorption. These effects facilitate chemical reactions by lowering activation barriers and increasing reaction rates. The synergy between hot carrier-induced redox reactions and thermocatalytic processes driven by localized heating allows for the activation of challenging reactions with reduced energy inputs. The balance between these pathways can be optimized through rational design of photothermal catalysts. In this review, we highlight recent advancements in catalyst materials, especially emphasizing the importance of photothermal effects to achieve higher efficiencies in CO_2 conversion reactions such as CO_2 hydrogenation and dry reforming of methane, both of which are vital for reducing greenhouse gases and producing clean fuels. Finally, the current challenges, outlook, and new strategies for catalyst optimization will be discussed to realize the full potential of photothermal catalysis in creating a sustainable and low-carbon energy future.

Keywords: Photothermal catalyst, plasmonic, carbon dioxide conversion, hydrogenation, dry methane reforming

INTRODUCTION

Carbon dioxide (CO_2) conversion into value-added chemicals and fuels is an essential strategy to transition towards a sustainable energy future[1-3]. The increasing levels of atmospheric CO_2 concentration require innovative approaches for carbon capture and utilization. Among the various techniques developed for CO_2 conversion, photothermal catalysis has emerged as a particularly promising method[4-8]. By harnessing both light and thermal energy, photothermal catalysts can drive chemical reactions under mild conditions, offering a synergistic effect that reduces operating temperature and enhances efficiency. This dual-energy approach enables reactions that are often more challenging or less efficient when using conventional thermal or photocatalytic methods independently.

One of the most studied reactions in photothermal CO_2 conversion is CO_2 hydrogenation, a process that reduces CO_2 to produce valuable hydrocarbons and alcohols, such as carbon monoxide (CO), methane (CH_4), and methanol[9-17]. Photothermal CO_2 hydrogenation benefits from the combined effects of light absorption and localized heating, which facilitates the activation of CO_2 molecules and their subsequent hydrogenation reaction with gaseous hydrogen (H_2). This reaction not only holds promise for producing clean fuels but also offers a pathway for integrating renewable solar energy into chemical processes. Recent advancements in catalyst design have significantly improved the efficiency and selectivity of photothermal CO_2 hydrogenation.

Another important photothermal CO_2 conversion catalysis is the dry reforming of methane (DRM). This reaction simultaneously converts two major greenhouse gases (CO_2 and CH_4) into syngas (a mixture of H_2 and CO), which serve as a precursor for various industrial chemicals and fuels[18-24]. In conventional thermocatalytic DRM, the reaction typically requires high temperatures of 700-900 °C, which are necessary to overcome the thermodynamic barriers. However, these harsh conditions pose several challenges, including the high energy input and the carbon coking on the catalyst surface, which leads to rapid catalyst deactivation. Photothermal catalysis offers a promising solution to these challenges by enabling DRM to proceed at significantly lower temperatures while maintaining high conversion efficiencies. Recent studies have shown that photothermal catalysts can mitigate carbon coking due to the photo-excited charge carriers and enhanced reaction kinetics.

This review will provide an in-depth examination of recent progress in photothermal catalysis, with a focus on two key CO_2 conversion reactions: CO_2 hydrogenation and DRM. We will introduce the underlying mechanisms that drive the enhanced catalytic activity observed in photothermal processes. This review also explores the latest advancements in catalyst materials, including the design of nanostructured and hybrid systems that have demonstrated superior performance. Finally, we will address the current challenges and perspectives, such as the need for a deeper understanding of the photothermal effects and the development of durable catalysts. Through this comprehensive review, we aim to provide future directions and opportunities for research in photothermal catalysis, emphasizing its potential to contribute to a low-carbon and sustainable energy future.

FUNDAMENTALS OF PHOTOTHERMAL CATALYSIS

Photothermal effects

Photothermal catalysis is an emerging field that combines light and thermal energy to drive chemical reactions with improved efficiency and selectivity. A key aspect of this approach is the photothermal effects, which involve converting absorbed photons into heat while simultaneously generating high-energy charge carriers, often called hot carriers. These photothermal effects arise from several interconnected processes, including plasmonic light absorption, hot carrier generation, photon-to-phonon conversion, local heating,

and heat transfer/dissipation [Figure 1]. Understanding these mechanisms is significant for designing effective photothermal catalysts for CO_2 conversion reactions.

Plasmonic light absorption

Plasmonic light absorption is the first and the most important step for photothermal catalysis, primarily occurring in metal nanoparticles (NPs) with free electrons [Figure 1A]. These NPs possess unique optical properties due to the collective oscillation of free electrons when exposed to light at specific wavelengths[25]. This resonance results in the strong absorption of light and the concentration of electromagnetic fields at the surface. The plasmonic resonance wavelength can be finely tuned by modifying the size, shape, and composition of the NPs, allowing for precise control over the light absorption spectrum due to factors such as surface scattering and radiation damping[26-28]. For instance, when the mean free path of conduction electrons becomes comparable to the particle size, there is increased electron-surface collisions and a blue shift in the surface plasmon resonance peak[29]. In contrast, when NPs get larger, they exhibit redshifts due to enhanced radiative losses and dynamic depolarization effects. The shape of NPs also plays a crucial role in determining plasmonic properties. For example, nanorods exhibit two surface plasmon resonance modes: a transverse mode and a longitudinal mode that shifts to longer wavelengths as the aspect ratio increases. Upon light absorption, plasmonic NPs transfer energy to free electrons, generating a non-equilibrium distribution of energetic electrons and holes, known as hot carriers.

Hot carrier generation and redox reactions

The absorption of light by plasmonic metal NPs leads to the generation of hot carriers (electrons and holes) which have energies significantly higher than the thermal equilibrium state. This process begins with the excitation of electrons to higher energy states within the conduction band, leaving behind corresponding holes in the valence band [Figure 1B]. Hot electrons generated through plasmonic excitation have energies that exceed the Fermi level of the metal, enabling them to overcome activation barriers for specific reactions[30,31]. For instance, in CO_2 reduction reactions, hot electrons can reduce CO_2 molecules adsorbed on the surface, while the corresponding hot holes can oxidize other reactants, completing the catalytic cycle. The direct involvement of hot carriers in redox reactions resembles conventional photocatalysis, where photo-excited electrons and holes in the semiconductors participate in redox reactions[32,33]. The lifetime and energy distribution of hot carriers are influenced by various factors, such as the size and shape of the plasmonic NPs and the properties of the surrounding medium. Hybrid materials that combine plasmonic metals with semiconductors are particularly effective because they facilitate charge separation, prolonging the lifetime of hot carriers and enhancing the ability to participate in catalytic reactions. In these materials, hot electrons can be injected into the conduction band of the semiconductor, while hot holes remain in the metal, enabling spatially separated redox processes[34,35].

Photon-to-phonon conversion and local heating

Not all the energy absorbed by plasmonic NPs is converted into hot carriers; most of the absorbed photon energy is dissipated as heat through photon-to-phonon conversion[36]. When hot carriers relax back to their equilibrium state, they release energy in the form of phonons, which are quantized vibrations of the crystal lattice [Figure 1C]. This energy release results in localized heating of the NP and its surroundings, leading to a rapid increase in temperature at the nanoscale[37,38]. Local heating is a key feature of photothermal catalysis and plays a vital role in enhancing reaction kinetics. Localized heating can enable the reaction to proceed under milder conditions, reducing the overall energy input. The extent of local heating depends on several factors, including the amount of absorbed photons, the thermal conductivity of the metal NPs and support materials, and the efficiency of heat dissipation to the surrounding environment[39,40].

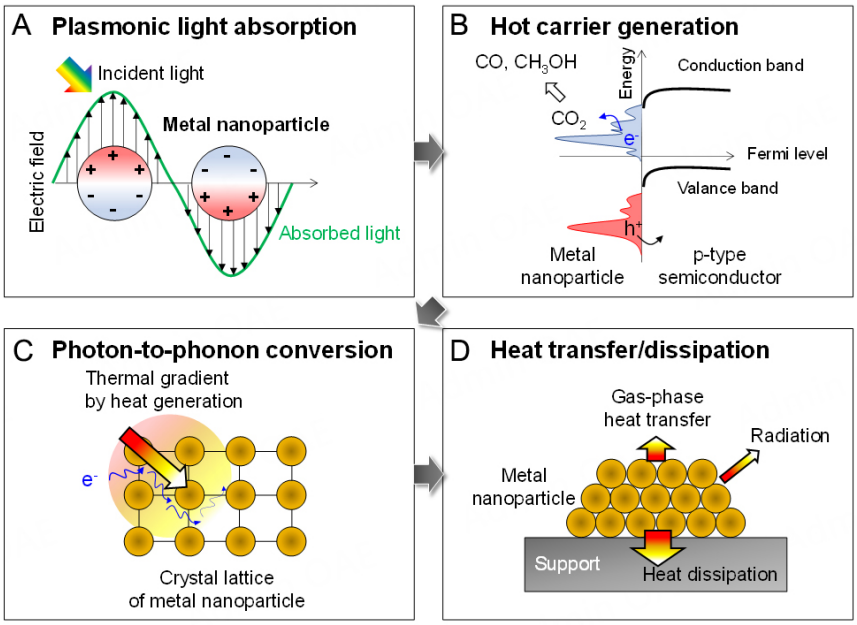

Figure 1. Key processes in the photothermal effect. (A) Light absorption at specific resonant wavelengths occurs through plasmonic excitation within metal nanoparticles, generating high-energy charge carriers. (B) Hot electrons (e^-) can directly participate in CO_2 reduction reactions when the metal nanoparticle forms a junction with a p-type semiconductor, while in n-type semiconductors, hot holes (h^+) can facilitate oxidation reactions. (C) Photon-to-phonon conversion within the crystal lattice of metal nanoparticles leads to localized heating. (D) The accumulated heat is subsequently transferred or dissipated to the surrounding environment or support material, contributing to a temperature gradient.

Heat transfer

Heat transfer is a critical aspect of photothermal catalysis, as it determines how the heat generated by photon-to-phonon conversion is distributed across the catalyst and the surrounding medium [Figure 1D]. For chemical reactions that require high temperatures, it is crucial to confine heat locally to maintain elevated temperatures. In contrast, efficient heat transfer is essential to maintain the desired reaction environment and prevent overheating of the catalyst working at low temperatures. In photothermal systems, heat can be transferred through conduction, convection, and radiation, with conduction being the primary mode at the nanoscale[41,42]. Design of photothermal catalysts must consider the thermal properties of both the active material and the support. Moreover, spatial distribution of heat within the catalyst can influence the selectivity of the reaction. In some cases, temperature gradients created by localized heating can drive specific reaction pathways, favoring the formation of desired products. To optimize heat transfer in photothermal catalysts, researchers have explored core-shell structures, where a plasmonic core is encapsulated by a shell material with tailored thermal properties[9,40,43,44]. For example, applying nanoporous oxide materials on top of the metal NPs can create a nanoscale greenhouse effect, achieving high local temperatures[9]. This design enables precise control over the thermal environment and can enhance the durability of the catalyst under operating conditions.

Interplay between photothermal effects and catalytic reactions

The integration of photothermal effects into catalytic reactions represents a promising strategy for enhancing reaction efficiency, productivity, and stability. When plasmonic NPs absorb light, they primarily generate two types of energy: hot carriers and thermal energy. These energies drive chemical reactions via two major pathways: hot carrier-induced redox reactions and thermocatalytic reactions facilitated by localized heating [Figure 2]. Understanding the interplay between these pathways is crucial for optimizing photothermal catalysis.

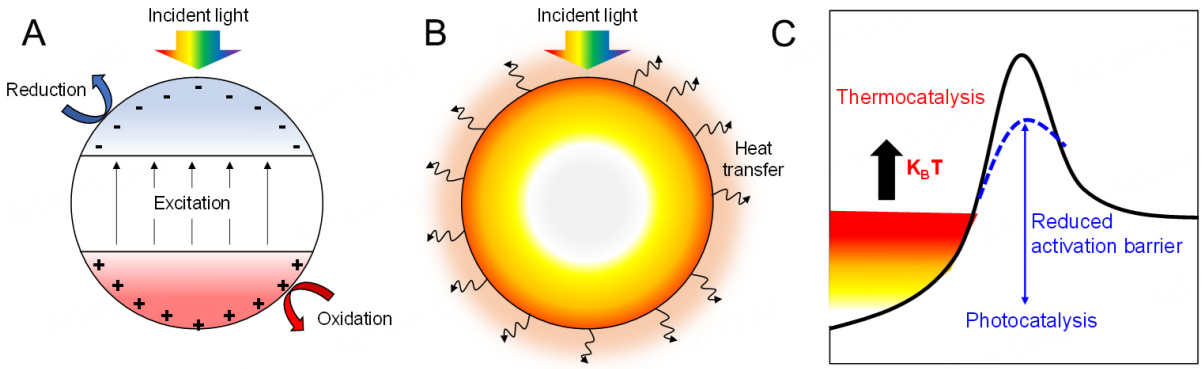

Figure 2. (A) Plasmonic photocatalysis driven by photo-excited hot charge carriers. (B) Plasmonic thermocatalysis driven by heat energy generated from solar light. (C) Reduction of activation energy barrier by local hot charge carriers (photocatalysis) and acceleration of thermocatalytic reaction kinetics due to Boltzmann thermal energy (K_BT) supplied to the reactants surrounding the plasmonic nanoparticle.

Hot carrier-induced redox reactions

When plasmonic NPs absorb light, the energy is transferred to free electrons, generating a non-equilibrium distribution of energetic electrons and holes, commonly referred to as hot carriers. These hot carriers can participate in driving redox reactions at the NP surface similar to conventional photocatalysis [Figure 2A]. Due to their high energy, hot carriers can overcome the activation energy barrier for electron transfer processes, facilitating reactions that would otherwise be thermodynamically unfavorable. The efficiency of this pathway depends heavily on the lifetime and energy of the hot carriers.

Thermocatalytic reactions driven by local heating

The photothermal effects generate localized heating through photon-to-phonon conversion. This thermal energy can drive thermocatalytic reactions, where the increase in temperature enhances the reaction rate by providing the necessary activation energy [Figure 2B][42]. The elevated local temperature can enhance the rate of bond cleavage and formation, leading to higher catalytic activity. The thermal effect also influences the kinetics of the reaction, often making the reaction pathway similar to traditional thermocatalysis. However, the localized and transient nature of the heating can lead to unique reaction dynamics that are distinct from conventional thermal catalysis.

Synergistic effects between hot carriers and thermal energy

The most compelling aspect of photothermal catalysis is the synergy between hot carriers and thermal energy, which together provide a dual enhancement to the catalytic process. When both pathways are engaged, the reaction can overcome the activation energy barrier through two complementary mechanisms [Figure 2C]. The first mechanism is related to the thermal effect, which increases the thermal energy of the system, often expressed as K_bT, where K_b is the Boltzmann constant and T is the absolute temperature. This thermal energy corresponds to the average kinetic energy of the reactant molecules. As the temperature rises, the kinetic energy of the molecules increases, leading to more frequent and energetic collisions between them. These higher-energy collisions provide sufficient energy to surpass the activation energy barrier. Secondly, the hot carriers can modify the electronic structure of the surface and induce electronic interactions that further reduce the activation barrier as photocatalytic reactions. This combined effect allows for the activation of otherwise challenging reactions, improving both the reaction rate and selectivity. The interplay between these effects creates a more favorable reaction environment, enabling reactions that require lower energy input compared to those driven solely by thermal or solar energy.

The interpretation of chemical reactions within the framework of photothermal catalysis depends on understanding the dominant energy source driving the reaction. If the absorbed light primarily generates hot carriers that directly participate in the reaction, the mechanism leans toward photocatalysis. On the other hand, if photon-to-phonon conversion predominates, leading to significant thermal energy generation, the reaction resembles traditional thermocatalysis. Identifying the major energy source for the reaction is critical for designing experiments and interpreting reaction pathways in photothermal catalysis research. Currently, most studies in the field focus on the thermal aspect, analyzing reaction mechanisms through thermocatalysis. This approach is reasonable, given the significant heat generated by plasmonic NPs during light absorption. However, the role of hot carriers cannot be disregarded, as they introduce unique reaction pathways that differ from classical thermocatalysis. The strategic design of materials and catalysts to optimize these effects is critical for advancing the field, particularly in applications such as photothermal CO_2 hydrogenation and DRM.

PHOTOTHERMAL CATALYST FOR CO_2 HYDROGENATION

CO_2 hydrogenation refers to the reaction between carbon dioxide and hydrogen to produce C1 or C2+ products. While numerous studies have been conducted on producing C2+ compounds, these reactions remain complex and require significant energy input, thus presenting several challenges[45]. Consequently, much of the research has focused on the production of C1 products, which serve as precursors for various industrial applications. The most prominent reactions in this field include CO_2 methanation, Reverse Water Gas Shift (RWGS) reaction, and methanol synthesis, which are respectively written as

$$CO_2 + 4H_2 \leftrightarrow CH_4 + 2H_2O \quad (1)$$

$$CO_2 + H_2 \leftrightarrow CO + H_2O \quad (2)$$

$$CO_2 + 3H_2 \leftrightarrow CH_3OH + H_2O \quad (3)$$

In these processes, CO_2 and H_2 are used as feedstocks, yielding CH_4, CO, and CH_3OH, respectively. By utilizing CO_2, a major greenhouse gas, these reactions offer significant environmental and industrial benefits by producing essential fuels and chemicals. Both photocatalytic and traditional thermal catalytic methods have been widely explored to facilitate these transformations. However, thermal catalysis requires substantial energy input and often suffers from catalyst deactivation due to coking at high temperatures[46]. Photocatalysis, on the other hand, is limited by its relatively low activity[47]. To address these challenges, there has been a growing emphasis on photothermal catalysis. Photothermal catalytic reactions demonstrate higher efficiency at lower temperatures compared to thermocatalytic processes[48] and gain attention due to their ability to harness abundant solar energy. Both precious metals and conventional transition metals have been utilized in the field of photothermal catalysts. Current research is focused on improving catalytic efficiency by optimizing light absorption and designing economically feasible catalysts. Additionally, many studies are dedicated to verifying the enhancement of photothermal effects through structural modifications of catalytic materials and further elucidating the mechanisms behind these effects.

Photothermal catalyst for CO_2 methanation

CO_2 methanation is a process in which CO_2 reacts with H_2 to produce CH_4, as given in:

$$CO_2 + 4H_2 \leftrightarrow CH_4 + 2H_2O \quad \Delta H_R^{298K} = -165 \text{ kJ mol}^{-1} \quad (4)$$

Recent studies for photothermal catalysts to produce methane are described below [Table 1].

Although CO_2 methanation is exothermic, the structural stability of CO_2 requires high temperatures of 300-400 °C for the reaction to proceed. Nickel (Ni) and ruthenium (Ru) catalysts are commonly utilized for this reaction, with nickel being particularly attractive due to its cost-effectiveness and efficiency[51,52,54]. However, at elevated temperatures, the methanation process often suffers from deactivation due to carbon deposition (coking) on the catalyst surface, along with competitive side reactions such as the RWGS reaction, leading to reduced efficiency[57]. Recent studies have focused on addressing these issues by targeting low-temperature methanation, with photothermal catalysis emerging as a promising approach. Photothermal catalysts leverage both light and heat to drive the reaction at lower temperatures, thereby improving energy efficiency using renewable energy sources such as solar power. Additionally, photothermal catalysis offers the potential to mitigate coking and enhance the long-term stability of the catalyst.

In 2022, Ge *et al.* focused on the development of Ru/H_xMoO_{3-y}, a catalyst synthesized via H_2-spillover to Ru/MoO_3 [Figure 3A]. The results show that the catalyst gained photothermal properties through the synthesis process[51]. The researchers studied the electrochemical and structural properties for the difference between Ru/H_xMoO_{3-y} and Ru/MoO_3. Ru/H_xMoO_{3-y} showed strong absorption of light with a wavelength of 500 to 800 nm, while Ru/MoO_3 hardly absorbed light with a wavelength over 400 nm [Figure 3B]. The researchers attributed the structural and electronic modifications to the H_2-spillover effect, in which Ru/H_xMoO_{3-y} forms oxygen vacancies and incorporates hydrogen atoms into the MoO_3 framework. These structural modifications affected the bandgap, enhancing the localized surface plasmon resonance (LSPR) effect [Figure 3C]. A significant increase in photocurrent density was observed compared to Ru/MoO_3 when visible (Vis)-near-infrared (NIR) light was applied, indicating the generation of photoinduced hot electrons [Figure 3D]. This effect was further validated through a CO_2 methanation reaction at room temperature. The Ru/H_xMoO_{3-y} catalyst achieved about 100% selectivity for methane using Vis and NIR light [Figure 3E]. Under Vis-NIR irradiation at a light intensity of 0.75 W cm^{-2} and 140 °C, the catalyst produced 20.8 mmol g^{-1} h^{-1} of methane, which was approximately 4.7 times higher than the 4.4 mmol g^{-1} h^{-1} achieved under dark conditions [Figure 3F]. However, the sample with 5 wt% Ru loading showed reduced light absorption and decreased catalytic activity, indicating that excessive Ru loading can negatively affect photothermal performance [Figure 3G]. The structural stability of Ru/H_xMoO_{3-y} was verified by comparing used samples with fresh ones, showing no significant changes in oxygen vacancies or surface conditions, demonstrating its robust structure. The study further revealed that the oxygen vacancies formed in Ru/H_xMoO_{3-y} could be regenerated during the reaction rather than disappearing, highlighting the catalyst's structure stability [Figure 3H]. Cycle tests confirmed the stability of the catalyst, although gradual decreases in photothermal activity were observed due to carbon deposition. The study conclusively demonstrated that the LSPR effect was significantly enhanced in Ru/H_xMoO_{3-y} that was prepared by utilizing H_2-spillover. The research illustrated that simple reduction treatment can induce both structural and electronic modifications, leading to enhanced photothermal effects and sufficient stability, making this catalyst an excellent candidate for further development.

In 2023, Guo *et al.* explored the use of heated substrates to enhance catalytic performance, beyond the widely studied LSPR effect of metal NPs[54]. They proposed that the heat generated through the non-radiative recombination of electrons could play a significant role in the reaction kinetics. In their study, $Ru/MnCo_2O_4$ catalysts were fabricated and evaluated based on the structural, redox, photothermal, and photoelectronic properties. The $Ru/MnCo_2O_4$ catalysts were compared with Ru/Al_2O_3 and Ru/TiO_2 catalysts, all sharing the same metal loading but differing in support materials. All three catalysts were synthesized

Table 1. Photothermal catalysts for CO_2 methanation

Product	Catalyst	m_{cat} (mg)	Flow rates (mL/min)	GHSV (mL/g·h)	Light source	Reaction condition (Photo energy in W/m^2)	Temp. (°C)	CH_4 production rate (mmol/g·h)	Pressure	Ref.
CH_4	$Ru_{0.88}Co_{0.12}/TiO_2$	50	20 (CO_2/H_2 = 1:4)	24,000	A 300 W Xe lamp (200 < λ < 1,100 nm)	Photothermal (19000)	300	191	1 bar	[49]
						Thermal	300	129.7		
	Ru/HNT	5	25 (CO_2/H_2 = 1:4)	300,000	a 300 W Xe lamp	Photothermal (20500)	350	1,704	1 bar	[50]
						Photothermal (5800)	250	4.5		
						Thermal	250	2.4		
	4%Ru/H_xMoO_{3-y}	150	10 (CO_2/H_2 = 1:1)	4,000	A Xe lamp (SAN-EI ELECTRIC XEF-501S) + 450 nm cut-off filter	Photothermal (7500)	140	20.8	1 bar	[51]
						Thermal	140	4.4		
	$CeNiO_3$	20	6 (H_2:CO_2 = 4:1)	18,000	300 W Xe lamp (PLS-SXE-300UV)	Photothermal (20000)	300	40	1 bar	[52]
						Thermal	300	18		
	$CeNiO_{3-x}$					Photothermal (20000)	300	80		
						Thermal	300	58		
	Ru/MnO_x	150	50 (CO_2/H_2 = 1:4)	20,000	full-arc A 300 W UV-Xe lamp	Photothermal (25000)	200	113.2	1 bar	[53]
						Thermal	200	7.2		
	Ru/$MnCo_2O_4$-2	50	20 (CO_2/H_2 = 1:4)	24,000	A 300 W Xe lamp (CEL-HXF300H5) (420 < λ < 780 nm)	Photothermal (12500)	230	66.3	1 bar	[54]
						Thermal	230	30.2		
	Ni/BN-4	20	2 (CO_2/H_2 = 1:4)	6,000	A 300 W Xe lamp (PLSSXE300D)	Photothermal	230	44.06	1 bar	[55]
						Thermal	230	0.64		
	Ni/TiO_2-25	10	25 (CO_2/H_2/He = 1:4:5)	150,000	a 300 W Xe lamp (PLS-SXE3000UV)	Photothermal (210000)	360	227.7	1 bar	[56]
						Thermal	360	45.2		

using the impregnation method. The increase in surface temperature under light irradiation was measured for each catalyst over time. The result showed that Ru/Al_2O_3 and Ru/TiO_2 achieved a maximum temperature of approximately 42 °C, whereas Ru/$MnCo_2O_4$ reached 85 °C and $MnCo_2O_4$ alone achieved 80 °C [Figure 4A]. This temperature increase was notably higher than that of MnO and Co_2O_3, confirming that $MnCo_2O_4$ can act as an efficient photothermal support, effectively converting light energy into thermal energy. Additionally, finite element simulations using COMSOL Multiphysics software demonstrated

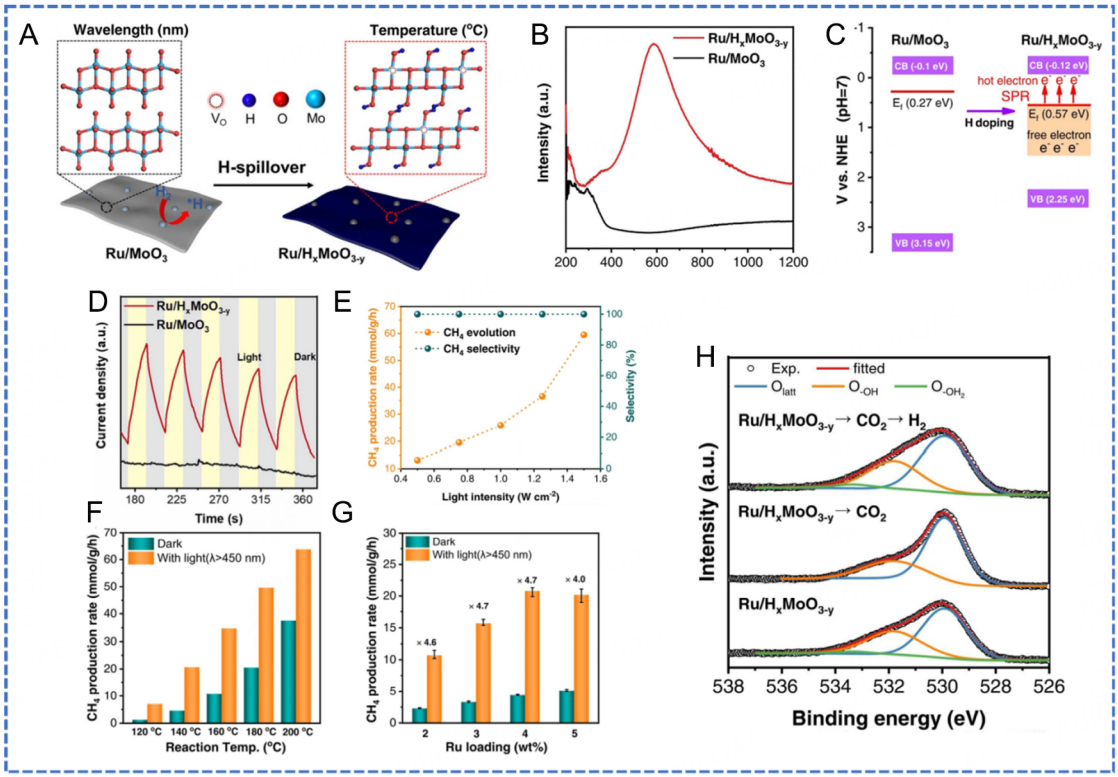

Figure 3. Properties and performance of Ru/H_xMoO_{3-y} and Ru/MoO_3. (A) Schematic of preparing for Ru/H_xMoO_{3-y} via H_2-Spillover using Ru/MoO_3. (B) UV-vis-NIR spectra absorption analysis of Samples. (C) Schematic of the band structure made based on analysis such as Tauc plots, VB XPS spectra, Mott-Schottky plots, *etc.* (D) Photocurrent density of samples under Vis-NIR light irradiation. (E) Methane production rate and selectivity depending on different light intensities. (F) Methane production rate with and without light at various temperatures. (G) Methane production rate with and without light for different Ru loading samples. (H) XPS spectra O 1s of Fresh sample, sample after CO_2 adsorption, sample reduced again by hydrogen after CO_2 adsorption. Reproduced with permission from Ref.[51].

that a stronger electric field was generated at the Ru/$MnCo_2O_4$ interface compared to Ru/TiO_2. This enhanced electromagnetic field amplified the photothermal effect, resulting in notable differences in CO_2 methanation performance [Figure 4B]. Under conditions of 12,500 W m^{-2}, light with wavelengths between 420 and 780 nm, and 200 °C, other catalysts exhibited methane production rates of 5-10 mmol g^{-1} h^{-1}, while Ru/$MnCo_2O_4$ achieved nearly 70 mmol g^{-1} h^{-1} [Figure 4C]. These results demonstrate that the photothermal support significantly increases methane production by reducing the activation energy under light irradiation [Figure 4D]. Performance evaluation based on metal loading revealed that excessive metal loading led to a decrease in activity due to NP agglomeration, reducing the number of available active sites [Figure 4E]. Thus, this study highlights that not only do metals with LSPR effects play a crucial role in photothermal catalysis, but the photothermal support itself can enhance the overall catalytic efficiency by intensifying the photothermal effect.

In 2024, Zhai *et al.* revealed that Ru combined with MnO_x plays a crucial role in photothermal CO_2 methanation[53]. MnO_2 was synthesized using a hydrothermal method, and Ru was anchored via photo-deposition. The catalyst exhibited increased CO_2 adsorption capacity and surface area, with Ru existing in a metallic state and reduced under light irradiation [Figure 5A]. The Ru/MnO_x catalyst, containing Mn^{4+}, Mn^{3+}, and Mn^{2+} [Figure 5B], achieved a CH_4 production rate of 113.2 mmol g^{-1} h^{-1} at 200 °C under a light intensity of 25,000 W cm^{-2}. The result was significantly more effective than the 7.2 mmol g^{-1} h^{-1} observed

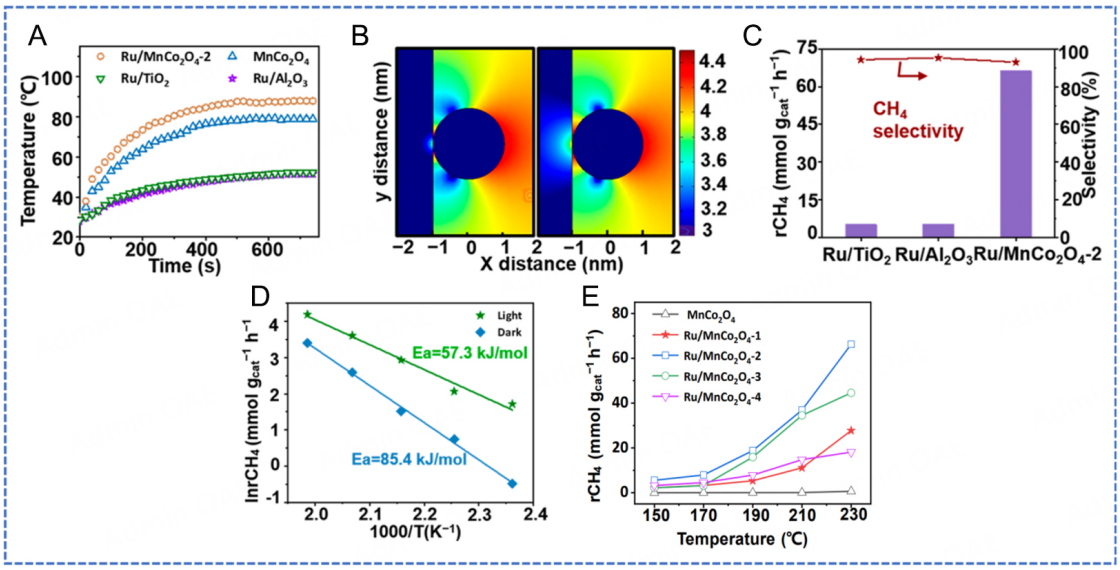

Figure 4. Properties and performance of $Ru/MnCo_2O_4$-X, Ru/TiO_2 and Ru/Al_2O_3, *etc.* (A) Temperature changes of $Ru/MnCo_2O_4$-2, $MnCo_2O_4$, Ru/TiO_2 and Ru/Al_2O_3 (50 mg of catalysts mixed with 1.2 g of quartz sands) under visible light irradiation (420-780 nm, 12,500 W m^{-2}) (B) Induced electric field distributions for Ru/TiO_2 and $Ru/MnCo_2O_4$ under light irradiation with a wavelength of 420 nm and intensity of 12,500 W m^{-2}. (C) production rate and selectivity for samples. (D) activity energy calculated with Arrhenius equation for CH_4 formation over $Ru/MnCo_2O_4$-2. (E) Methane production rate for different Ru loading samples at various temperatures. Reproduced with permission from Ref.[54].

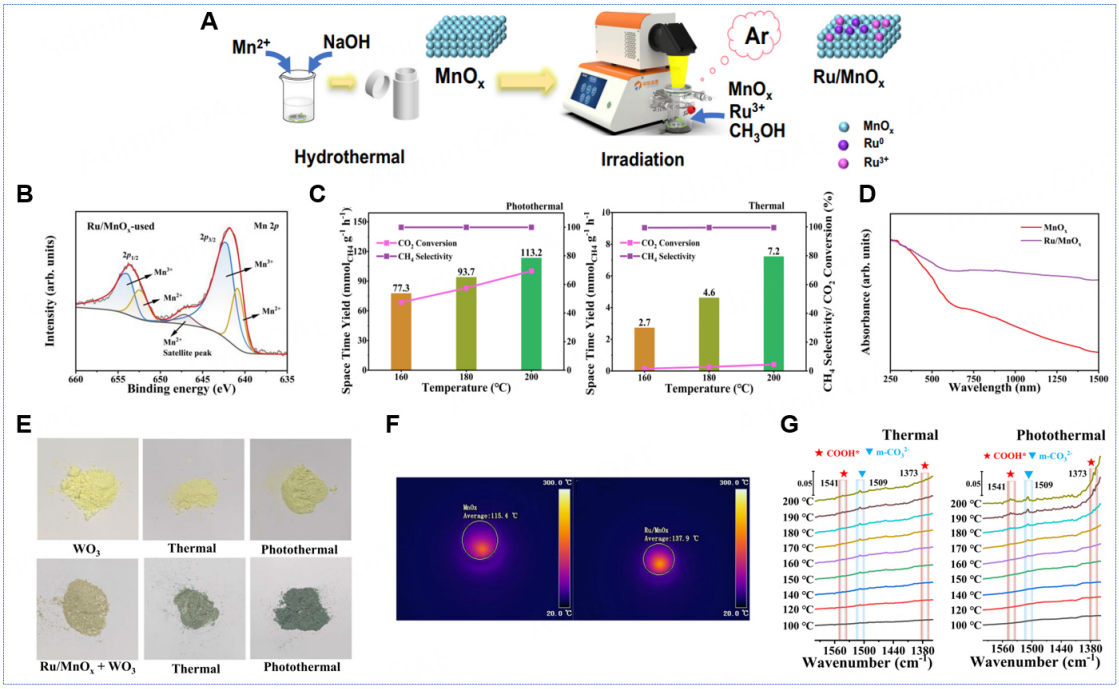

Figure 5. Preparation diagram and properties of Ru/MnO_X and MnO_X (A) Schematic of the synthesis procedure of Ru/MnO_X. (B) Mn 2p: XPS spectra of MnO_X. (C) Production rate with and without irradiation depending on temperature. (D) UV-vis-IR spectra absorption analysis of MnO_X and Ru/MnO_X. (E) Photographs of WO_3 and the mixture of WO_3 and Ru/MnO_X after reduction, thermal reaction and photothermal reaction. (F) Infrared thermal images for MnO_x and Ru/MnO_x under light with intensity about 2.5 W cm^{-2}. (G) FT-IR analysis of Ru/MnO_X at thermal and photothermal condition. Reproduced with permission from Ref.[53].

under dark conditions at the same temperature [Figure 5C]. Ru enhances the H_2-spillover effect, resulting in structural changes and strong absorption from ultraviolet (UV) to NIR wavelengths, making the photothermal methanation reaction more efficient [Figure 5D]. The H_2-spillover effect of Ru was further demonstrated using WO_3 support which readily reacts with hydrogen and darkens upon reaction. Although WO_3 alone showed little color change, the catalyst mixed with Ru/MnO_x and WO_3 darkened significantly under thermal conditions and became even darker under photothermal conditions. This observation demonstrates that H_2-spillover effect of Ru is more effective under light irradiation. Additionally, when Ru was added to MnO_x, the catalyst displayed broad and strong light absorption from UV to NIR wavelengths [Figure 5E]. The surface temperature under light irradiation was approximately 22 °C higher than in samples without Ru [Figure 5F]. This clearly demonstrates that Ru not only induces structural changes but also plays a crucial role in the photothermal reaction. Notably, the Ru/MnO_x catalyst promotes the formation of COOH intermediates in the CO_2 methanation reaction. The COOH intermediate is a key step in the production of CH_4, and the photothermal catalyst significantly reduces the activation energy, thus enhancing reactivity [Figure 5G]. This catalyst also exhibits high efficiency in both CO_2 adsorption and H_2 dissociation, achieving a CH_4 selectivity of up to 99.5%. In addition, Ru/MnO_x maintained high activity and stability during long-term reactions under photothermal conditions. This performance was particularly efficient in CH_4 production, yielding better results under photothermal conditions compared to thermal conditions. This study highlights the crucial role of Ru in various aspects of photothermal reaction for CO_2 methanation.

In summary, various metals (Ru, Ni, Co, *etc.*) have been used as catalysts for photothermal CO_2 methanation. Recently, Ru has been regarded as the optimal metal for achieving catalytic activity at low temperatures, despite its high cost. The studies demonstrate that Ru effectively activates hydrogen at low temperatures. Researchers also focus on whether the photothermal effect can be enhanced using different supports. The synergy between the metal and support has been shown to enhance the photothermal effect, which positively impacts the CO_2 methanation reaction. These results suggest that the synergy between metal catalysts with appropriate supporting materials could further enhance the potential for developing cost-effective catalysts.

Photothermal catalyst for reverse water gas shift (RWGS) reaction

The RWGS reaction involves the conversion of CO_2 and H_2 into CO and water (H_2O), as given in:

$$CO_2 + H_2 \leftrightarrow CO + H_2O \quad \Delta H_R^{298K} = 41 \text{ kJ mol}^{-1} \tag{5}$$

The RWGS reaction is one of the most prominent processes for producing CO, which serves as a crucial feedstock for the synthesis of various chemical products. Transition metal catalysts such as Cu[58], Ni[56], Fe[59], and Co[60], along with precious metals such as Pt[61], and Rh[62], are commonly utilized in this reaction, with support materials such as ceria (CeO_2)[48] and titania (TiO_2)[63] enhancing catalytic performance. Since the RWGS reaction is inherently endothermic, it requires high reaction temperatures to proceed efficiently, typically above 400 °C[64]. However, such high temperatures often lead to catalyst deactivation primarily due to the formation of carbon deposits (coking) on the catalyst surface, which significantly diminishes catalytic activity. Efforts to address these challenges have led to extensive research into optimizing catalyst compositions, support materials, and reaction conditions. Despite these studies, the development of catalysts capable of maintaining high activity and stability under high-temperature conditions remains a critical challenge. As a result, photothermal catalysts have garnered significant attention for their ability to utilize both light and heat, enabling high efficiency at lower temperatures while also mitigating coking. Current research on photothermal catalysts in the RWGS reaction focuses on key areas such as low-

temperature activation, enhancing the photothermal synergy effect, understanding catalyst-support interactions, suppressing coking, and elucidating the underlying reaction mechanisms. These advancements aim to achieve a more efficient and economically viable CO_2 conversion process. Recent studies for RWGS reaction are being conducted for use in industry. A summary of these recent studies is provided below [Table 2].

In 2020, Guo *et al.* developed an effective catalyst for RWGS reaction using economical and environmentally friendly materials[58]. They used hydroxyapatite [HAP, $Ca_{10}(PO_4)_6(OH)_2$] [Figure 6A], a material known for its simplicity in synthesis and scalability and its widespread use in various fields due to its eco-friendly properties. Additionally, copper (Cu) is abundant and cost-effective while possessing strong hydrogen activation properties. They synthesized Cu-HAP ($Cu_xCa_{10-x}(PO_4)_6(OH)_2$) by substituting calcium in HAP with copper for RWGS reaction. Light irradiation allowed Cu-HAP to achieve higher activity compared to the dark experiment. For the photothermal reaction, a light intensity of approximately 20,000 W m^{-2} was used, and the catalyst's photothermal activation was observed without any external heat supply. The catalytic activity significantly increased in the high-temperature range, starting from 120 °C and rising to 300 °C. The performance was approximately 2 to 3 times higher under light than without light in the flow reactor [Figure 6B]. The copper loading was varied from 0% to 100% and then evaluated for the RWGS performance. Notably, the catalyst with 10% copper exhibited optimal performance and reducibility. The catalyst achieved a CO_2 conversion rate of approximately 60% and nearly 100% selectivity toward CO [Figure 6C]. The reducibility is explained by the dispersion of copper. Even when synthesized using tap water, the catalyst demonstrated minimal performance variation, emphasizing the simplicity and practicality of the synthesis method [Figure 6D]. Moreover, the surface area remained stable even after calcination, ensuring long-term stability of the catalyst [Figure 6E]. Additionally, the research team extensively evaluated and analyzed the synthesized, calcined, and reduced forms of the catalyst to elucidate the mechanism by which the Cu-HAP catalyst operates as a photothermal catalyst. It was confirmed that metallic Cu NPs formed during the reduction process significantly enhanced catalytic activity through the photothermal effect. These results demonstrate that the Cu-HAP catalyst exhibits photothermal catalytic properties and can play a crucial role in industrial-scale CO_2 reduction and CO production. One of the most significant aspects of this study is the economic feasibility of the catalyst, which can be produced at a cost of approximately $1 per kilogram [Figure 6F]. The research demonstrates that the catalyst meets the four essential criteria for industrial applications: abundance of raw materials, simplicity of synthesis, low production cost, and non-toxicity. Cu-HAP catalysts are expected to be widely used in industrial applications given these advantages.

In 2021, Deng *et al.* synthesized a highly dispersed Ga-Cu/CeO_2 catalyst using a metal-organic framework (MOF) template[48]. They demonstrated the role of Ga and Cu in promoting the RWGS reaction. The researchers synthesized a CeO_2-based MOF, then prepared the Ga-Cu/CeO_2 catalyst via an ion-exchange method. The key finding of this study was the significant improvement in Cu dispersion in MOF-derived catalysts compared to those made using typical wet impregnation methods. Specifically, the 10Cu5Ga/CeO_2-w catalyst prepared by wet impregnation exhibited a low dispersion of 16.1%, while the MOF-derived samples, 10Cu/CeO_2 and 10Cu5Ga/CeO_2, achieved much higher dispersion of 49.2% and 47.4%, respectively. This result emphasizes the advantage of the MOF-templated synthesis method in enhancing metal dispersion, which significantly improves catalytic performance. The researchers also evaluated the photothermal properties of the CeO_2-based catalysts by monitoring temperature changes under light irradiation. The addition of Cu greatly enhanced the photothermal heating efficiency of the catalyst, whereas the addition of Ga had minimal impact on heat generation [Figure 7A]. However, a significant difference in CO production rates was observed between the Ga-doped and non-doped samples.

Table 2. Photothermal catalysts for RWGS

Product	Catalyst	m_{cat} (mg)	Flow rates (mL/min)	GHSV (mL/g·h)	Light source	Reaction condition (Photo energy in W/m^2)	Temp. (°C)	Syngas production rate (mmol/g·h)	Pressure	Ref.
Syngas	Au/CeO_2	50	3 (CO_2:H_2.N_2 = 1:4:95)	3,600	Xe lamp (PLS-SXE300, visible light)	Photothermal (32000)	400	0.64	1 bar	[65]
						Thermal	400	0.05		
	6.3 Pd/TiO_2	50	20 (CO_2:H_2 = 1:4)	24,000	300 W Xe lamp (CEL-HXF300-T3) + NIR light (400 < λ < 1,100 nm)	Photothermal (25000)	250	7.4097	1 bar	[63]
						Thermal	250	0.4128		
	In_2O_{3-x}/In_2O_3	20	1 (CO_2:H_2 = 1:1)	3,000	a 300 W Newport Xe lamp	Photothermal (~8 suns.)	300	2.051	1 bar	[66]
						Thermal	300	0.363		
	10 mol% Cu-HAP	10	2 (CO_2:H_2 = 1:1)	12,000	A 300 W Newport Xe lamp	Photothermal (20000)	300	1.34	1 bar	[58]
						Thermal	300	0.48		
	Co_{15}HAP	100	26 (CO_2:H_2 = 1:1)	15,600	150 W Xe lamp	Photothermal (1080)	400	62	1 bar	[67]
						Thermal	400	58		
						Photothermal (1080)	250	16		
						Thermal	250	3		
	10Cu5Ga/CeO_2	10	20 (CO_2:H_2 = 1:1)	120,000	A LA-251 Xe lamp with a HA30 filter was utilized as UV-vis irradiation source A 300 W Xenon arc lamp	Photothermal (UV-vis light)	320	54.8	1 bar	[48]
						Thermal	320	36		
						Photothermal (19520)	285	111.2		
	$CuCo_5BO_x$	20	50 (CO_2:H_2 = 4:1)	150,000	A 300 W xenon lamp	Photothermal (5000)	300	124.7	1 bar	[68]
						Thermal	300	35		
	Rh/TiO_2 -2	50	20 (CO_2:H_2 = 1:4)	2,000	a 300 W Xe lamp (200 < λ < 1,100 nm),	Photothermal (27000)	250	20.6	1 bar	[62]
						Thermal	250	1.8		

This synergy between Cu and Ga significantly increased CO production rates under photothermal conditions, with the optimized 10Cu5Ga/CeO_2 catalyst achieving a CO production rate of 111.2 mmol g^{-1} h^{-1} and nearly 100% selectivity under the maximum light irradiation [Figure 7B]. They revealed that Ga enhances catalytic activity through mechanisms beyond the heat generation induced by light. Mechanistic studies indicated that Ga doping promotes the

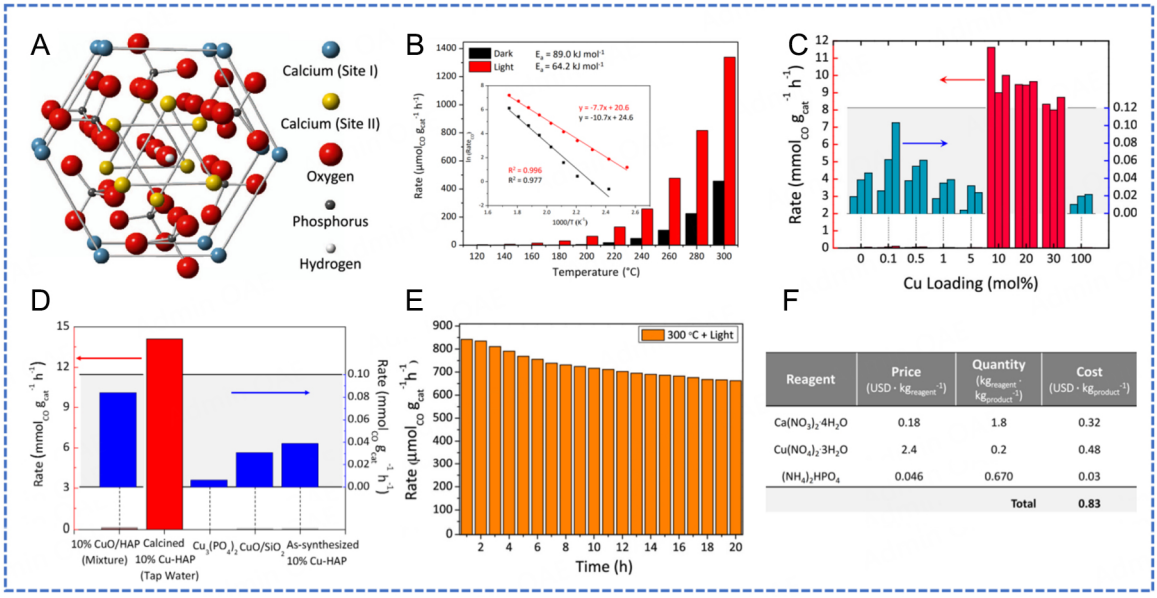

Figure 6. Model of HAP structure and activity test for catalysts. (A) Crystal structure of hydroxyapatite. (B) Methane production rate with and without light at various temperatures and Arrhenius plot. (~2.0 W cm^{-2} light intensity, H_2:CO_2 ratio 1:1, flow rate = 2 sccm). (C) The CO production rate of Cu-HAP depended on the Cu loading amount. (D) RWGS activities of various samples in the batch reactor. (E) Duration test of 10% Cu-HAP at 300 °C under light irradiation. (F) In bulk industrial, price and quantity for synthesis of catalysts are used for RWGS reaction. Reproduced with permission from Ref.[58].

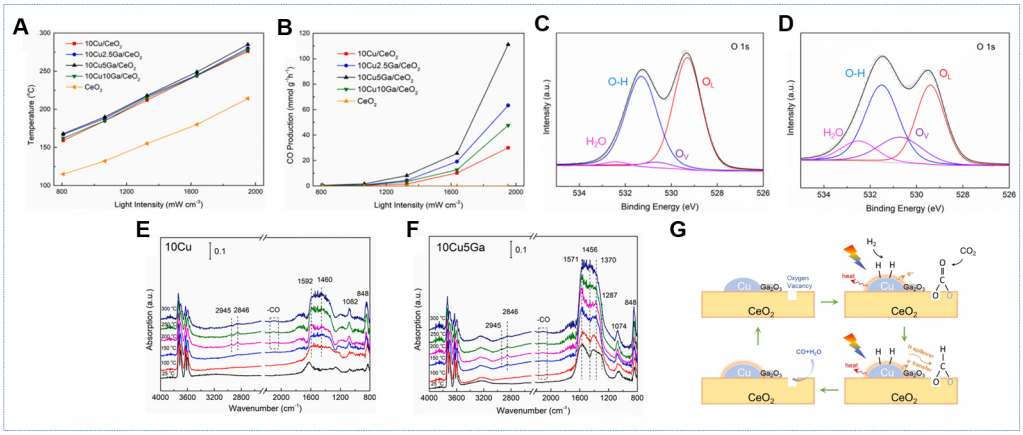

Figure 7. Structure-property analysis, activity test and mechanism study for samples. (A) Light intensity-dependence of temperature for samples supported on CeO_2 different loadings of Cu and Ga. (B) Light intensity-dependence of CO production rate for samples with different loadings of Cu and Ga on CeO_2. (C) O 1s: XPS spectra of 10Cu/CeO_2. (D) O 1s: XPS spectra of 10Cu5Ga/CeO_2. (E) *in situ* DRIFTS spectra analysis over 10Cu/CeO_2 during photothermal RWGS reaction. (F) Over 10Cu5Ga/CeO_2. (G) Schematic of photothermal RWGS reaction mechanism for catalyst supported Cu and Ga. Reproduced with permission from Ref.[48].

formation of oxygen vacancies, which serve as active sites for CO_2 adsorption by increasing the reducibility of the catalyst [Figure 7C and D]. Additionally, *in situ* diffuse reflectance infrared transform spectroscopy (DRIFTS) analysis confirmed that Ga promotes the formation of key intermediates, such as formates, which are crucial for CO_2 hydrogenation [Figure 7E and F]. In summary, this study highlighted the complementary roles of Cu and Ga within the catalyst system. Cu primarily contributes to the photothermal effect and facilitates the H_2-spillover mechanism, while Ga enhances the reducibility of the CeO_2 matrix, increasing the number of available CO_2 adsorption sites. The use of the MOF-templated synthesis method

underscores its potential for producing highly dispersed metal catalysts, demonstrating an approach that significantly improves RWGS catalytic performance under photothermal conditions. This study emphasizes Ga's critical role in modulating the electronic structure of the catalyst, promoting oxygen vacancy formation, and facilitating key reaction intermediates [Figure 7G].

Previous studies have emphasized the importance of dispersion. It was known well that particle size is closely related to dispersion[69]. In 2023, Yang *et al.* examined how the catalytic activity varies with the size of Pd metal particles[63]. In general, catalytic activity changes depending on the size of metal NPs. In this study, they synthesized catalysts with particle sizes of 2.8, 3.4, 4.7, 5.3, 6.3, and 8.1 nm [Figure 8A]. They conducted reaction experiments from 50 to 250 °C to analyze the effect of particle size on catalytic performance. The results showed that activity increased with larger particle sizes but began to decrease beyond a certain particle size [Figure 8B]. They suggested that precisely controlling the size of Pd NPs can modify SMSI (Strong Metal Support Interaction). This alteration changes the electronic properties, significantly affecting catalytic performance. To evaluate the metal-support interaction, they analyzed binding energy. The binding energy followed a similar trend to the change in activity based on particle size. In a reaction experiment under irradiation at an intensity of 2.5 W cm^{-2} and a temperature of 250 °C, the production rate reached 7.4097 mmol g^{-1} h^{-1}, while under dark conditions, it was only 0.4128 mmol g^{-1} h^{-1}, showing a considerable difference [Figure 8C]. The turnover frequency (TOF) of 6.3Pd/TiO_2 was approximately 800 min^{-1}, followed by 5.3Pd/TiO_2 with around 600 min^{-1} [Figure 8D]. These results indicate that changes in the metal-support interaction and electronic properties modulation due to particle size have a substantial impact on catalytic performance. In this study, SMSI was used to explain the significant charge transfer in the reaction. Another study shows that another dopant can further promote charge transfer.

In 2024, Wang *et al.* presented a study where boron-oxide (B-O) was identified as a key component in the $CuCo_5BO_x$ catalyst, enhancing photothermal catalytic performance through increased CO_2 adsorption capacity and improved charge transfer[68]. The $CuCo_5BO_x$ catalyst exhibited an amorphous $CoBO_x$ structure with coexisting Cu^0 and Cu^+ crystalline phases. Boron was well incorporated into the catalyst lattice, contributing to an increased specific surface area, thereby optimizing the reaction efficiency [Figure 9A]. The researchers reported that the primary roles of B-O are enhancing CO_2 adsorption and accelerating charge transfer, both of which were found to be crucial for the catalyst's enhanced performance [Figure 9B]. Comparative studies between Cu-Co, $CuCo_5B$, $CuCo_5O_x$, and $CuCo_5BO_x$ catalysts demonstrated that the boron-doped catalyst exhibited superior CO_2 adsorption, a trend consistent with its enhanced catalytic activity [Figure 9C]. Furthermore, the charge transfer ability of B-O was investigated through a series of photochemical characterizations, including measurements of photocurrent density for $CuCo_5O_x$ and $CuCo_5BO_x$ catalysts [Figure 9D]. This revealed a distinct improvement in electron transfer with the boron-containing catalyst, supporting its role in boosting photothermal reactions. The $CuCo_5BO_x$ catalyst achieved a remarkable production rate of 124.7 mmol g^{-1} h^{-1} at 300 °C, with a selectivity of approximately 97%. This is nearly three times the performance of thermal catalysts at the same temperature [Figure 9E]. After 10 h of reaction at 300 °C, a slight decrease in yield was observed; however, the catalyst retained its morphology, crystalline structure, and chemical state, demonstrating excellent stability. Additionally, the catalyst maintained a high production rate of 88.1 mmol g^{-1} h^{-1} even after one year of storage, confirming its potential for long-term stability and reusability [Figure 9F].

Photothermal catalyst for methanol synthesis reaction

The reaction for synthesizing methanol from CO_2 and H_2 can be written as follows:

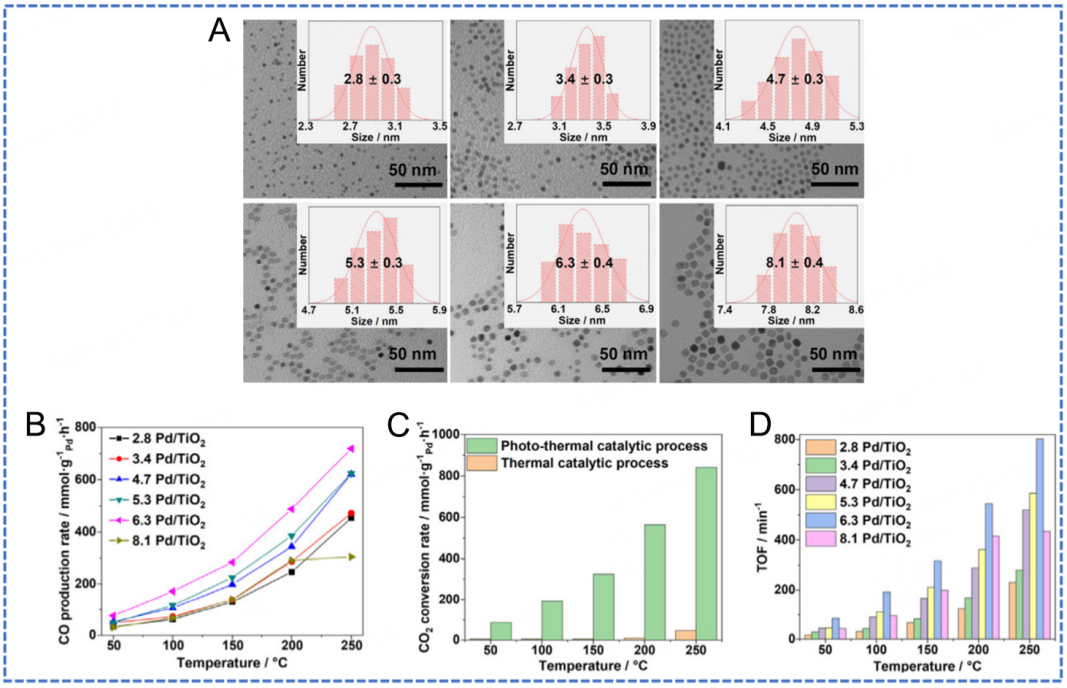

Figure 8. Particle size and activity test for catalysts. (A) TEM images of catalysts with different particle sizes. (B) Temperature-dependence of CO production rate for samples with different loadings of Pd on support. (C) CO_2 conversion rate at various temperatures in photothermal and thermal reactions. (D) Turnover frequency number for CO production on catalysts in photothermal reaction. Reproduced with permission from Ref.[63].

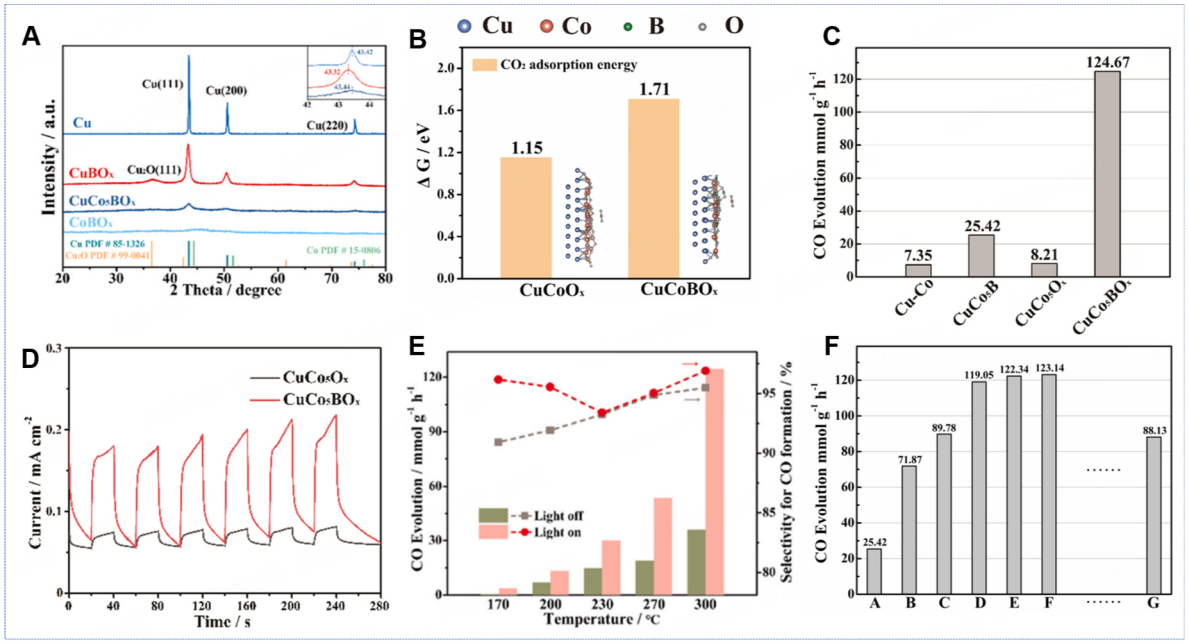

Figure 9. Activity test results and properties analysis of catalysts. (A) XRD graphs of Cu, $CuBO_X$, $CuCo_5BO_X$, and $CoBO_X$ (B) The CO_2 adsorption energy of samples. (C) The reaction test of various catalysts (Reaction condition: 20 mg weight, 300 °C reaction temperature, 50 W m^{-2} light intensity. (D) Photocurrent density of $CuCo_5O_X$ and CuCo5BO_X. (E) CO production rate with and without light at various temperatures. (F) CO production rate of samples treated at different conditions (A: vacuum drying for 12 h; B: dry in the air at 25 °C for 4 h G: leave at room temperature for one year). Reproduced with permission from Ref.[68].

$$CO_2 + 3H_2 \leftrightarrow CH_3OH + H_2O \quad \Delta H_R^{298K} = -49\ kJ/mol^{-1} \tag{6}$$

Methanol is an important chemical compound with a high energy density, making it highly valuable in the chemical industry as a fuel, solvent, and chemical intermediate. The synthesis of methanol from CO_2 is a crucial approach for sustainable carbon utilization, with catalysts such as Cu, Ru, Ni, and Pd being commonly utilized. Among these, Cu is widely used due to its low cost and relatively high selectivity. However, Cu-based catalysts exhibit their highest efficiency under harsh conditions, typically requiring high temperatures (200-300 °C) and pressures (3-10 MPa)[70]. These severe conditions can reduce the overall energy efficiency of the process and impact the durability of the equipment in industrial applications. Additionally, since methanol synthesis is an exothermic reaction, it can promote RWGS reaction, leading to the production of unwanted CO, which in turn decreases methanol selectivity[71]. To overcome this issue, catalyst design must focus on suppressing the RWGS reaction while enhancing methanol selectivity. To address these challenges, recent research has focused on the development of catalysts that can efficiently promote methanol synthesis under ambient pressure. Photothermal catalysis has emerged as a promising strategy for methanol synthesis, utilizing both light and heat to drive the reaction under milder conditions. This approach shows great potential by enabling effective catalytic performance even at lower temperatures and ambient pressure, thereby increasing the commercial viability of CO_2-to-methanol conversion. However, the low reaction rate of photothermal catalysts is a significant barrier to commercial applications. Moreover, the long-term stability of photothermal catalysts remains a concern as catalytic performance tends to degrade over time. Recent studies for photothermal catalysts to produce methanol are presented below [Table 3].

In 2018, Wang *et al.* confirmed that the previously reported $In_2O_{3-x}(OH)_y$ catalyst plays a crucial role in the RWGS reaction by facilitating the conversion of CO_2 to CO. This study also explored the potential of $In_2O_{3-x}(OH)_y$ as a promising catalyst for methanol production[77]. The group found that Surface Frustrated Lewis Pairs (SFLP) formed on the catalyst surface promotes hydrogen dissociation, which plays a vital role in methanol synthesis. They reported that the In···InOH bond, combined with SFLP and extended charge carrier lifetime, enhances hydrogen dissociation. This effect is amplified when light is applied, directly contributing to the improved activity of the catalyst. Although no structural differences were observed between the samples, the increased length of the nanorods extended the charge carrier lifetime, thereby maximizing reaction efficiency. This highlights the importance of charge transport and dissociation in enhancing catalytic performance. The study also investigated the physical properties of the catalyst, particularly the effect of nanorod length on catalytic activity. As the synthesis time increased, the length of the nanorods also grew. The lengths of the nanorods synthesized for 3, 9, and 14 h were 950, 1,685, and 2,580 nm, respectively. Although the surface area of the catalyst synthesized for 3 h was slightly lower, other physical properties exhibited minimal variation across the samples. Methanol selectivity consistently remained between 53% and 60% across all samples, but differences in catalytic activity were observed. Under solar irradiation, catalytic activity increased significantly with longer synthesis times, achieving rates of 14.09, 54.04, and 97.3 μmol g^{-1} h^{-1} for the 3, 9, and 14-h samples, respectively [Figure 10A]. This suggests that the synergistic effect of charge carrier lifetime and nanorod length is a critical factor in enhancing catalytic performance. In terms of stability, the catalyst initially showed a high production rate of 97 μmol g^{-1} h^{-1}, which decreased to 55 μmol g^{-1} h^{-1} over time. However, after 15 h, the production rate increased again, and stabilized at 64 μmol g^{-1} h^{-1}, demonstrating strong long-term stability [Figure 10B]. Selectivity remained consistent at around 50% throughout the reaction, further proving the catalyst's stability and reliable performance [Figure 10C]. The study suggests that further research is needed to investigate the effect of SFLP on catalytic activity in detail. A deeper understanding of this mechanism could lead to the design of more efficient catalysts for methanol production.

Table 3. Photothermal catalysts for synthesis MeOH

Product	Catalyst	m_{cat} (mg)	Flow rates (mL/min)	GHSV (mL/g·h)	Light source	Reaction condition (Photo energy in W/m^2)	Temp. (°C)	MeOH production rate (mmol/g·h)	Pressure	Ref.
MeOH	Cu/ZnO	20	20 (CO_2:H_2 = 1:3)	60,000	LA-251Xe lamp (420 < λ < 800 nm)	Photothermal (5800)	220	0.1278	1 bar	[72]
						Thermal	220	0.0828		
	2Ru/In_2O_3	10	20 (CO_2:H_2 = 1:3)	120,000	LA-251 Xe lamp, (400 < λ < 800 nm)	Photothermal (6442)	250	0.178	1 bar	[73]
						Thermal	250	0.1228		
	CZA	30	20 (CO_2:H_2 = 1:3.2)	40,000	a LX300F Xe (350 < λ < 800 nm)	Photothermal (6000)	225	7.8125	21 bar	[74]
						Thermal	225	5.9375		
	Pd/ZnO	100	34 (CO_2:H_2 = 1:3)	20,400	two 500 W high-pressure mercury lamps	Photothermal	250	3.8	12 bar	[75]
						Thermal	250	0.8		
	10% Ni-In_2O_3	100	20 (CO_2:H_2 = 1:3)	12,000	AM 1.5G filter and a 300W Xenon lamp	Photothermal	265	1.9812	10 bar	[76]
						Thermal	265	1.16875		
	$In_2O_{3x}(OH)_y$-14 NR	15	8 (CO_2:H_2 = 1:3)	32,000	A Newport 130 W Xe arc lamp	Photothermal	250	0.0973	1 bar	[77]
						Thermal	250	0.0541		
	$H_zIn_2O_{3-x}(OH)_y$	N/A	4 (CO_2:H_2 = 1:1)	N/A	a 300 W Xe lamp (PLS-SXE300D)	Photothermal	300	0.01895	1 bar	[78]
						Thermal	300	0.02303		

In 2019, Wang *et al.* developed a Cu/ZnO catalyst and conducted extensive examination on how hot electrons generated by visible light influence methanol synthesis[72]. The Cu to Zn molar ratio was set at 1:2, and the catalyst was prepared using the co-precipitation method. When comparing the light absorption characteristics of ZnO and Cu/ZnO, a distinct absorption peak was observed at 584.3 nm, attributed to the Cu NPs [Figure 11A]. This led to an improvement in production rate from 1.38 to 2.13 μmol g^{-1} h^{-1} under light irradiation [Figure 11B]. They claimed that the reduction in activation energy by 40% in the presence of Cu NPs demonstrated that the reaction was promoted by hot electrons generated through Localized Surface Plasmon Resonance (LSPR) [Figure 11C]. They also extensively examined the mechanisms of both thermal and photothermal catalysis, confirming the impact of hot carriers. In thermal catalysis, *HCOO species adsorbed on ZnO, CH_3O species, and *HCOO species adsorbed on Cu followed the formate pathway. The reaction pathway did not change after irradiation. Instead, the hot carriers generated from Cu prevented the accumulation of *HCOO species on the surface, increasing the reaction rate during photothermal catalysis [Figure 11D]. This research offers the first extensive examination of the mechanism behind methanol synthesis at atmospheric pressure via photothermal catalysis. It seems clear that copper and Zn oxide play a beneficial role in methanol production. However, the role and synergy of each metal and metal oxide in photothermal reactions will be discussed in the next section.

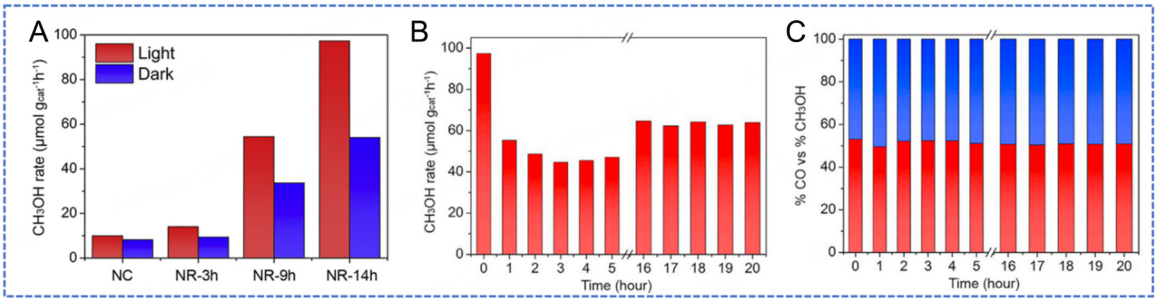

Figure 10. Performance test of catalysts. (A) MeOH production rate with and without light at various temperatures. (B) MeOH production rate during 20 h. (C) MeOH selectivity of the $In_2O_{3-X}(OH)_y$, NR-14h. Reproduced with permission from Ref.[77].

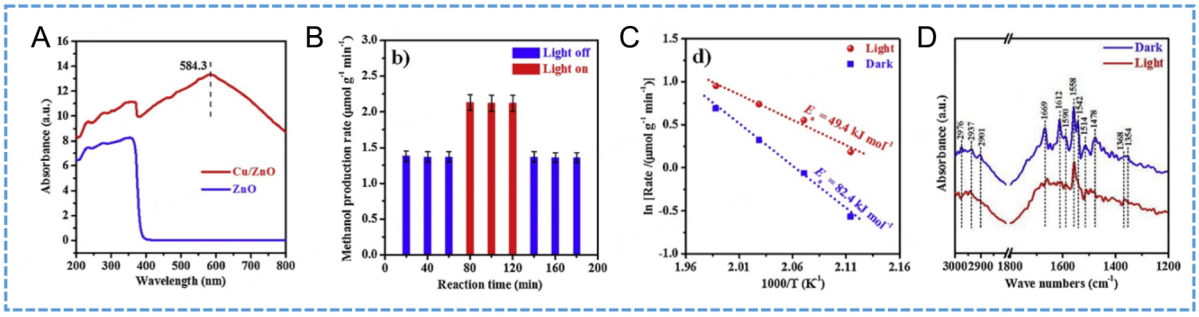

Figure 11. Properties and reaction mechanism study of CZ. (A) UV-vis spectra absorption analysis of CZ and ZnO. (B) MeOH production rate at 220 °C in visible light off and on. (C) activity energy under dark and light conditions calculated using Arrhenius equation for MeOH formation over CZ. (D) *in situ* DRIFTS spectra with and without light. Reproduced with permission from Ref.[72].

In 2020, Xie *et al.* conducted a detailed investigation into the roles of Cu and ZnO sites in the CZA ($Cu/ZnO/Al_2O_3$) catalyst[74]. The synergy between these roles maximized the activity of the CZA catalyst. Under light irradiation in the 350-800 nm range, at 21 bar and 225 °C, the CZA catalyst achieved a production rate of 7.8125 mmol g^{-1} h^{-1}, compared to 5.9375 mmol g^{-1} h^{-1} in dark conditions [Figure 12A]. Upon analyzing the catalytic activity under different light ranges, the production rate significantly increased within the 350-800 nm range, while no significant change in activity was observed within the 420-800 nm, 200-500 nm ranges. This indicates that specific wavelengths do not promote photothermal catalysis [Figure 12B]. The activation wavelengths for Cu and ZnO are different, and their simultaneous activation plays a crucial role. To further clarify the roles of Cu and ZnO, the research team conducted experiments using three catalysts: CZA, ZA (Zn/Al_2O_3), and CA (Cu/Al_2O_3). This study revealed that CO_2 adsorbs onto ZnO to form HCOO under visible light, which then reacts with adsorbed hydrogen (H) on Cu(I) species to produce methanol. The critical interface for this reaction is the boundary where hydrogen from Cu reacts with *HCOO adsorbed on ZnO. In the site where Cu is present alone, an increase in CO production was observed, reducing methanol selectivity [Figure 12C]. This suggests that controlling the catalyst composition is a key factor in enhancing selectivity in the CO_2-to-MeOH conversion reaction. Thus, this research not only provides a clear understanding of the individual roles of Cu and ZnO but also presents a new perspective on how the structure and morphology of catalysts can promote important reaction mechanisms [Figure 12D and E]. Ultimately, the study demonstrates that controlling composition and structure in catalyst design is essential to maximize methanol production.

In 2023, Deng *et al.* developed a Ru/In_2O_3 catalyst that significantly improved methanol production rates and highlighted the critical role of photothermal effects in enhancing catalytic performance[73]. The Ru/In_2O_3

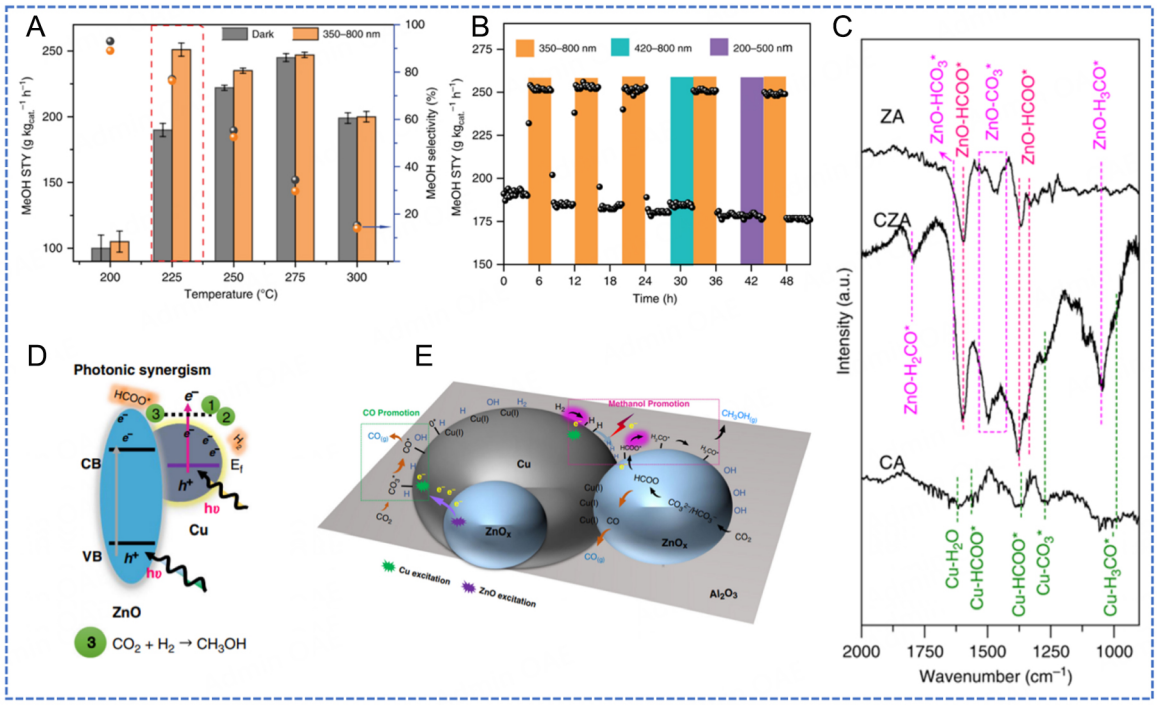

Figure 12. Production rate and selectivity of MeOH; Schematic of reaction mechanism for CZA. (A) Production rate and selectivity of MeOH over CZA with and without irradiation depending on temperature. (B) Methanol production rate of CZA as irradiated with different wavelengths of light. (C) The DRIFTS spectra of CZA, ZA and CA (D and E) Proposed schematic of CO_2 hydrogenation for synthesis MeOH over CZA. Reproduced with permission from Ref.[74].

catalyst demonstrated not only superior production rates compared to samples using other metals (Cu, Rh, Pt, Pd) but also achieved a selectivity of approximately 35% [Figure 13A]. The concentration of oxygen vacancies increased with higher Ru loading despite similar surface areas [Figure 13B-D]. The photothermal effect involves two key characteristics: the heating substrate effect and the generation of hot carrier electrons. A comparison between 290 °C in dark conditions and 280 °C under light irradiation showed a higher production rate at 280 °C with light irradiation, indicating that the enhancement in production was primarily because of hot carriers rather than thermal substrate heating [Figure 13E]. The analysis of the reaction mechanism suggested that the CO pathway dominated the reaction rather than the formate pathway as seen in other studies. In the overall process, the interaction between ruthenium and In_2O_3 increased the concentration of oxygen vacancies, providing more adsorption sites for CO_2. Subsequently, hydrogen spillover from Ru facilitated CO_2 activation, leading to the adsorption of *COOH, which was then converted to *CO. The combined effects of thermal substrate heating and hot carrier electrons promoted the accumulation of *CO, which was hydrogenated to produce methanol [Figure 13F]. This study effectively demonstrated the superior activity of Ru/In_2O_3 compared to other metal-based catalysts. The overall mechanism was shown to be a synergistic result of photothermal heating substrate effect and hot carrier-induced activation caused by Ru [Figure 13G]. Research on methanol production has been less extensive so far compared to RWGS and methanation. Methanol synthesis has many limitations compared to the other two reactions due to its complex mechanism and harsh reaction conditions.

PHOTOTHERMAL CATALYSTS FOR DRY REFORMING OF METHANE WITH CARBON DIOXIDE

PGM-based catalytic materials

PGM-based catalysts, such as those containing Pt, Rh, and Ru, have been widely investigated for their

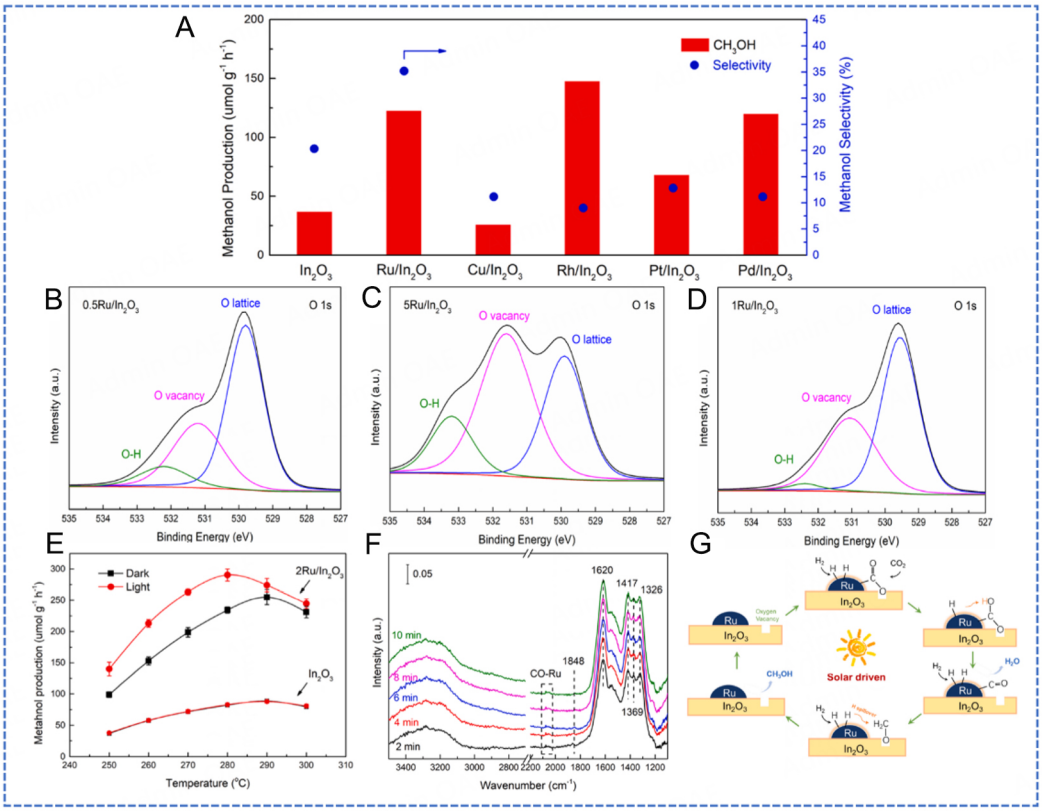

Figure 13. (A) MeOH production rate of catalysts supported on In_2O_3 for synthesis MeOH under dark conditions: 10 mg of catalyst, 250 °C, 1 bar, CO_2/H_2 = 5/15 mL min^{-1}. (B) O 1s: XPS spectra of 0.5Ru/In_2O_3. (C) O 1s: XPS spectra of 1Ru/In_2O_3. (D) O 1s: XPS spectra of 5Ru/In_2O_3. (E) MeOH production rate of Ru/In_2O_3 and In_2O_3 with and without light at different temperatures. (F) *in situ* DRIFTS for synthesis methanol over 2Ru/In_2O_3 at 200 °C (G) Schematic of synthesis MeOH over Ru/In_2O_3. Reproduced with permission from Ref.[73].

superior performance in photothermal DRM [Table 4]. Tang *et al.* reported that Ru/$SrTiO_3$ catalysts efficiently combine photothermal heating with electronic interactions between Ru and $SrTiO_3$, resulting in enhanced activation of CO_2 and CH_4 under light irradiation[19]. Similar to this, Hu *et al.* developed Ru_{SA+NP}/TiO_2, where the synergistic interaction between single-atom Ru sites and NPs not only improved light absorption but also enhanced catalytic stability during prolonged DRM operations[82]. Another approach by Shoji *et al.* highlighted the potential of Rh/$SrTiO_3$ catalysts, which utilize LSPR effects to overcome reaction barriers and achieve high syngas yields[22]. Also, Liu *et al.* demonstrated that Pt/TaN catalysts benefited from the light-induced local heating effects provided by the TaN support, significantly improving CH_4 conversion rates[84]. Together, these studies illustrate a diverse range of strategies to pave the way for more efficient and sustainable catalytic systems for DRM. We will now highlight a selection of key studies in this field to further explore the innovative advancements contributing to this PGM-based DRM catalyst.

In 2020, Zhou *et al.* reported the development of a Cu-Ru single-atom alloy plasmonic photocatalyst designed for the light-driven DRM reaction[18]. The conceptual catalyst structure developed here consists of Cu NPs acting as the light-absorbing antenna with single-atom ruthenium sites functioning as the active catalytic reactor sites [Figure 14A]. The term "light-absorbing antenna" refers to the role that Cu NPs play in capturing and concentrating light energy during the reaction. Single Cu NPs undergo a phenomenon called LSPR when exposed to light particularly in the visible range. This occurs when the light waves interact with the free electrons in the copper particles, causing them to oscillate. These oscillations amplify

Table 4. Summary of photothermal catalysts for dry reforming of CH_4 with CO_2

Catalyst	m_{cat} (mg)	Flow rates (mL/min)	GHSV (mL/g·h)	Light source	Reaction condition (Photo energy in W/m^2)	Temp. (°C)	CH_4 rxn rate (μmol/g·s)	H_2/CO ratio	Ref.
$Cu_{19.8}Ru_{0.2}$/MgO-Al_2O_3	1.5	16 (50% CH_4, 50% CO_2)	640,000	Supercontinuum laser (Fianium, WL-SC-400-8)	Photothermal (192,000)	RT	275	1	[18]
					Thermal	727	60	0.22	
Ni/mesoporous TiO_2	200	48 (21% CH_4, 29% CO_2)	14,400	Xenon light (XE-300F)	Photothermal (3.1)	RT	0.6	1	[79]
					Thermal	500	4.5	0.58	
					Photothermal (3.1)	500	7.9	0.65	
0.29 wt.% Ru/$SrTiO_3$	150	45 (36% CH_4, 36% CO_2)	18,000	A 300-W xenon lamp	Thermal	350	0.6	0.48	[19]
					Photothermal	350	4.7	0.61	
					Thermal	500	11.8	0.7	
					Photothermal	500	26.7	0.8	
SCM-Ni/SiO_2	25	118.7 (11.7% CH_4, 11.5% CO_2)	285,000	A 500 W Xe lamp (CHF-XM500)	Photothermal (343,600)	RT	154	0.86	[20]
(Ni/CeO_2)@SiO_2	25	50 (30% CH_4, 30% CO_2)	120,000	300 W Xenon lamp (CEL-HXF300)	Thermal	600	90	0.62	[80]
					Photothermal	600	143	0.62	
1.5Ni/SiO_2	30	20 (48% CH_4, 48% CO_2)	40,000	300 W Xe lamp (CEL-PE300E-3) with a concentrator	Photothermal (90000)	RT	28	0.45	[21]
					Thermal	700	80	0.64	
					Photothermal (90000)	700	188	0.86	
0.7Ni-0.8Co/SiO_2					Photothermal (90000)	RT	15.3	0.29	
					Thermal	700	9.4	0.23	
					Photothermal (90000)	700	145	0.80	
25 wt.% Ni/SiO_2	300	200 (10% CH_4, 12.5% CO_2)	40,000	a 300 W Xe lamp (Cermax PE300BUV) with a focusing lens (LGQ30/40P)	Photothermal	RT	4.6	0.59	[81]
Ru_{SA+NP}/TiO_2	2.5	20 (10% CH_4, 10% CO_2)	480,000	full-spectrum light, 300 W Xe lamp	Thermal	400	26	0.5	[82]
					Photothermal (28000)	400	45	0.63	
					Thermal	500	118	0.7	
					Photothermal (28000)	500	160	0.77	

10 wt.% $Rh/SrTiO_3$	5	10 (2% CH_4, 2% CO_2)	120,000	150 W Hg-Xe lamp (LA-410UV-5)	Photothermal	RT	8.7	1	[22]
$Rh/CeWO_3$	50	50 (20% CH_4, 20% CO_2)	60,000	A Xe lamp (CEL-HXF300 from CEAULIGHT, 300-1000 nm)	Thermal	300	1.9	0.9	[83]
					Photothermal (18000)	300	3.5	0.7	
Pt/TaN	100	20 (50% CH_4, 50% CO_2)	12,000	LA-251Xe lamp (Hayashi)	Thermal	500	3.3	0.88	[84]
					Photothermal (560)	500	4.5	0.92	
Mo_2C	120	20 (16.7% CH_4, 16.7% CO_2)	30,000	-	Thermal	900	45	0.5	[23]
				Xenon lamp	Photothermal (30,000)	RT	0.01	0.3	
				A fiber optic laser system (LSF20D, Hgtech laser)	Photothermal (20 W, 20 KHz)	RT	2200	0.95	
0.76 wt% Ni_{SA}/CeO_2	25	20 (20% CH_4, 20% CO_2)	48,000	300W Xe lamp (PLS-FX300HU)	Thermal	470	5.3	0.5	[85]
					Photothermal (24,000)	470	18	1	
CoNiRuRhPd /$SrTiO_3$	5	20 (10% CH_4, 10% CO_2)	240,000	300 W xenon lamp (PLS-XE300)	Thermal	500	1.7	0.9	[86]
					Photothermal (40,000)	RT	11	1	
Ni-CeO_2-$CePO_4$	N/A	10 (25% CH_4, 25% CO_2)	N/A	Prizmatix LEDs	Thermal	350	1.5	0.45	[87]
					Photothermal (48,100)	350	7.2	1	
Ru/TiO_2-H_2	5	50 (8% CH_4, 8% CO_2)	600,000	300 W Xe lamp (PLS-XE3000UV)	Thermal	400	0	N/A	[88]
					Photothermal (120,000)	400	70	0.9	
Ni/Ga_2O_3	40	20 (20% CH_4, 20% CO_2)	30,000	CEL-HXF300 from CEAULIGHT	Thermal	500	1.3	0.55	[89]
					Photothermal (30,000)	500	1.6	0.95	
Rh/Al_2O_3	230	50 (10% CH_4, 12.5% CO_2)	13,000	300 W Xe lamp (Cermax PE300BUV)	Photothermal (780)	RT	0.3	0.65	[90]
Pt/TiO_2	20	20 (48% CH_4, 48% CO_2)	60,000	Xenon lamp	Thermal	500	23	0.26	[91]
					Photothermal (42,000)	500	107	0.65	
1% Rh_2O_3 /Ga_2O_3	94	10 (48% CH_4, 48% CO_2)	6,400	300 W Xe lamp	Thermal	500	1.2	0.14	[24]
					Photothermal	500	1.8	0.22	
Pt/TNT	20	30 (5% CH_4, 5% CO_2)	90,000	300 W Xe lamp (PLS-SXE 300+)	Photothermal (35,000)	300	20	0.97	[92]

the local electromagnetic field near the surface of the NPs. When multiple Cu NPs are arranged in close proximity, the LSPR effect can be amplified due to interactions between the electromagnetic fields of neighboring particles. This interaction leads to the formation of "hot spots" where the local electromagnetic field is much stronger than in areas without such interactions. This is similar to how a traditional radio antenna amplifies a signal by adjusting its size and position relative to the incoming waves. Theoretically, by controlling the distance between Cu NPs and their relative distribution, the LSPR effect can be tuned to control light absorption characteristics of the photothermal catalyst. In this regard, several catalysts were synthesized by adjusting the ratio of Cu to Ru using co-precipitation on a $MgO-Al_2O_3$ composite support. Under focused white light illumination (19.2 W cm^{-2}), this photocatalyst demonstrated remarkable efficiency and stability at room temperature, eliminating the need for high temperatures (700-1,000 °C) typically required for DRM. The study achieved a turnover frequency of 34 mol H_2 per mol Ru per second, and the catalyst was stable for over 50 h of operation without noticeable coke formation [Figure 14B]. Previous studies on bimetallic plasmonic photocatalysts such as Au-Pd and Au-Pt have been limited by reduced photocatalytic activity due to the attenuation of plasmon resonance caused by high Pd or Pt loading. In addition, these systems have been faced with coking problems, which leads to catalyst deactivation. However, Cu-Ru single-atom alloys overcome these limitations by optimizing the catalyst structure. The researchers found that individual dispersion of ruthenium atoms on the surface of Cu NPs retained plasmonic activity and enhanced catalytic performance. The combination of hot carriers generated from Cu NPs and single-atom Ru active sites significantly reduced the energy barrier for methane decomposition which leads to a more efficient reaction with an excellent H_2:CO (1:1) ratio [Figure 14C]. The paper also showed that the catalyst resists coking, which is attributed to the isolated nature of Ru atoms preventing carbon accumulation. This group also tries to explain the high H_2:CO ratio with DIET (Desorption Induced by Electronic Transitions) mechanism that can quickly remove the adsorbed H atoms on surfaces, which will be further discussed later.

In 2022, Yang *et al.* reported Rh-based catalyst design for photothermal DRM that dispersed on Ce-W mixed oxide support[83]. They focused on efficiently combining photothermal and photoelectric effects. Rh NPs (NPs) are uniformly dispersed on the Ce_xWO_3 nanosheets synthesized by a solvothermal method [Figure 15A]. The prepared Rh/Ce_xWO_3 catalyst exhibited high activity toward DRM under mild conditions, achieving H_2 and CO production rates of 88.5 and 152.3 mmol g_{Rh}^{-1} h^{-1}, respectively, at the light intensity of 1.8 W cm^{-2} without external heating [Figure 15B]. The unique aspect of this catalyst is the metal-metal charge transfer (MMCT) process. Irradiation induces charge transfer between Ce and W atoms, thereby promoting the redox cycle that enhances oxygen mobility. The authors suggested that this enhanced oxygen mobility helps remove precipitated carbon and improve catalyst activity and stability over multiple cycles. Compared to typical DRM catalysts, the Rh/Ce_xWO_3 catalyst operates at much lower temperatures due to the synergistic effects of photothermal and photoelectrochemical processes. The MMCT between Ce and W lowers the activation energy of the reaction, which enhances the efficiency and stability of the catalyst [Figure 15C]. Moreover, the design of the Ce_xWO_3 support with hexagonal tungsten bronze (HTB) structure helps to remove carbon deposits by increasing oxygen mobility. This is a significant improvement over other supports such as Rb_xWO_3 which do not show the same level of catalytic performance. The catalyst achieves a high photochemical energy efficiency of 4.65%, which outperforms previously reported photocatalysts under similar conditions. The key finding of this work is the importance of oxygen mobility in the support material, particularly the Ce_xWO_3, which can do prevent coking and promote DRM process. The ability of oxygen to migrate through the lattice and interact with deposited carbon is crucial for retaining the catalyst's stability.

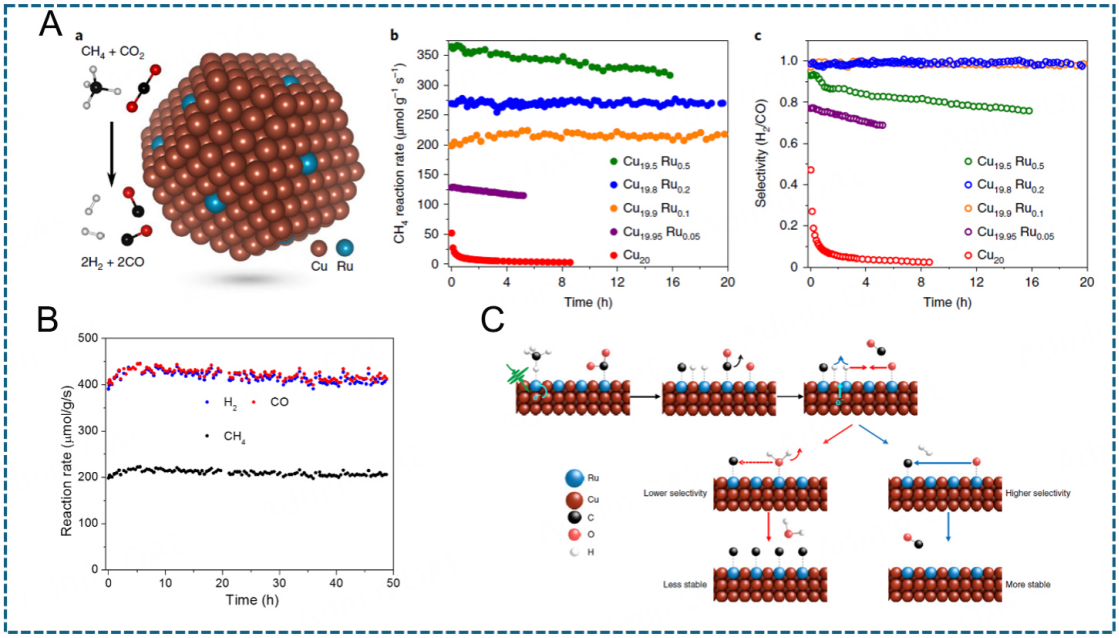

Figure 14. Dry reforming of methane reaction catalyzed by platinum group metal (PGM)-based photothermal catalytic materials: (A) Schematic of a Cu-single-atom Ru surface alloy catalyst with the dry reforming reactants and products. Reaction rate and long-term stability and selectivity of photocatalytic DRM over CuRu alloy catalyst. (B) Stability of photocatalytic methane dry reforming reaction on a $Cu_{19.9}Ru_{0.1}$ sample under 19.2 W·cm^{-2} white light illumination. (C) Schematics of enhanced selectivity and stability in photocatalysis via the DIET mechanism. Reproduced with permission from Ref.[18].

In 2023, Li *et al.* emphasized the significance of modulating strong metal-support interaction (SMSI) to improve the light-driven DRM reaction using Ru/TiO_2 catalyst [Figure 16A][88]. They explored how SMSI can affect the electron transfer between Ru NPs and TiO_2 support to suppress the catalytic activity in photothermal reactions. They prepared two variants of Ru/TiO_2 catalysts, one with suppressed SMSI effect (Ru/TiO_2-H_2) and the other with normal SMSI effect (Ru/TiO_2). Here, Ru/TiO_2-H_2 was prepared simply by pre-reducing TiO_2 under H_2 before impregnating Ru on it. The Ru/TiO_2-H_2 catalyst exhibited significantly improved performance, with 46 times higher CO_2 conversion than the typical Ru/TiO_2 catalyst [Figure 16B]. The study explains that this performance difference is due to the ability of the Ru/TiO_2-H_2 catalyst to better facilitate electron transfer to surface oxygen vacancies, thereby promoting CO_2 activation and improving methane decomposition step.

In 2024, He *et al.* reported a method to precisely control dispersed platinum species on TiO_2 nanotube support[92]. They designed a series of catalysts containing both single-atom Pt sites and sub-nanoclusters of Pt on the TiO_2 nanotube surface [Figure 16C]. These Pt species were carefully controlled via a spatially confined approach, which ensured highly dispersed Pt species and prevented agglomeration. The researchers obtained various compositions of Pt species by changing the calcination conditions. The most optimized catalyst, consisting of a mixture of Pt single-atom and sub-nanoclusters, exhibited a syngas production rate of 34.41 mol g_{Pt}^{-1} h^{-1} and an apparent quantum yield of 9.1% at a wavelength of 365 nm under photothermal conditions at 300 °C. The major improvement of this work over previous photothermal DRM lies in the synergistic interaction between Pt single sites and Pt sub-nanoclusters. Single-atom catalysts are known for their high atom utilization efficiency but often struggle with bimolecular reactions such as DRM due to the lack of active sites. On the other hand, Pt sub-nanoclusters provide a larger number of active sites but tend to incur undesirable side effects such as excessive CO adsorption. By combining both single atoms and sub-nanoclusters, the researchers created a balance where single atoms activate CH_4 while

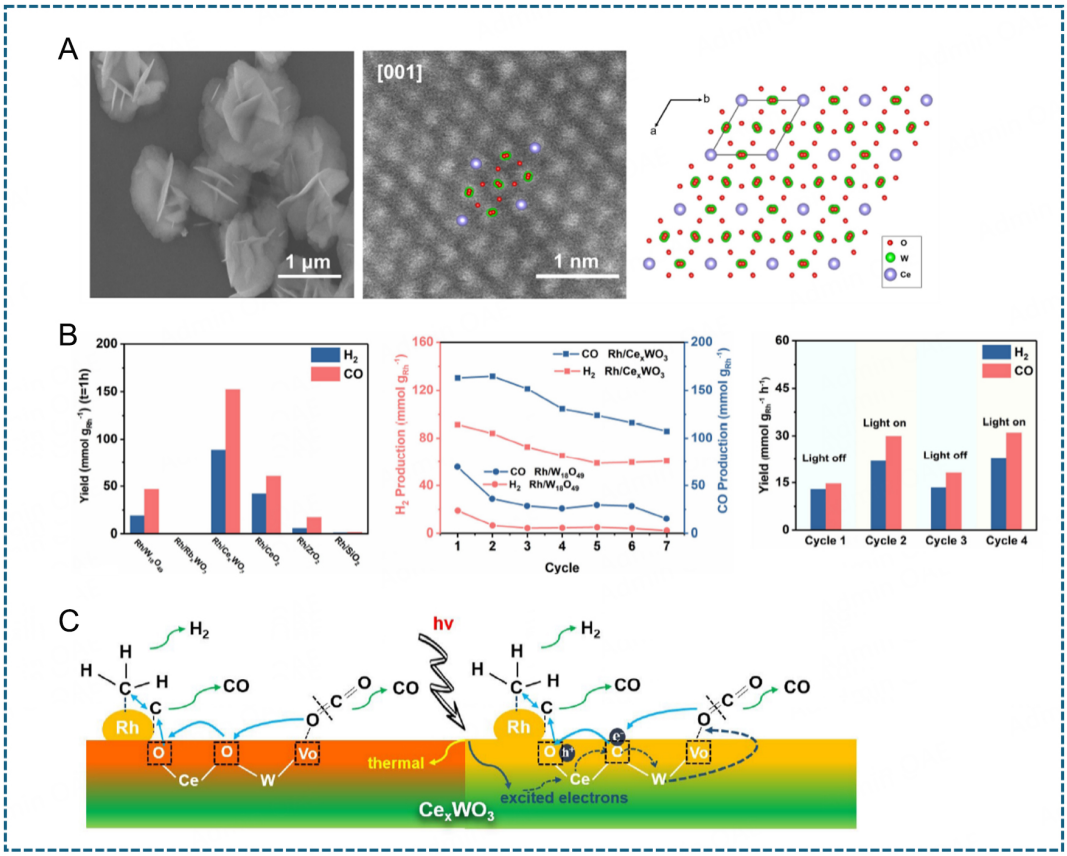

Figure 15. Dry reforming of methane reaction catalyzed by platinum group metal (PGM)-based photothermal catalytic materials: (A) A SEM image and high-resolution HAADF-STEM image of as-prepared Ce_xWO_3 and a unit cell of Ce_xWO_3 projected along c axis was superimposed on it. (B) Rates of H_2 and CO produced using different samples in a batch reactor and cycle experiments of DRM over Rh/Ce_xWO_3 catalyst in a batch reactor. Rates of H_2 and CO at 300 °C with and without irradiation in a flow reactor (gas flow rate: 50 mL min^{-1}, 1 atm). (C) Schematic diagram for light-driven DRM reaction over Rh/Ce_xWO_3 catalyst. Reproduced with permission from Ref.[83].

sub-nanoclusters activate CO_2, leading to a better performance in DRM reaction. In the same year, Xiong *et al.* reported the development of a high-entropy alloy (HEA) catalyst composed of five different metals including Co, Ni, Ru, Rh, and Pd supported on $SrTiO_3$ as an effective photocatalyst for DRM reaction [Figure 16D][86]. The combination of these metals results in a uniform solid solution without phase separation. This uniformity ensures that the active sites on the catalyst surface are well-dispersed, preventing aggregation and providing high exposed area of all kinds of metal atoms. The authors claimed that the HEA catalysts utilize a carbon exchange mechanism where carbon atoms from methane and CO_2 are exchanged, while oxygen atoms circulate between CO_2 and the lattice oxygen of $SrTiO_3$. The HEA catalyst exhibited excellent DRM performance in producing H_2 and CO at rates of 15.6 and 16.0 mol g_{metal}^{-1} h^{-1}, respectively [Figure 16E]. The catalyst achieved long-term stability over an operating period of more than 150 h, maintained high selectivity, and suppressed undesirable side effects such as the RWGS pathway. Another feature of HEA catalyst is its broad light absorption range from UV to near infrared. This enables facile photothermal reaction without external heating by raising local surface temperatures. As shown in these works introduced above, researchers are focusing on selecting the most effective PGM (Pt, Rh or Ru) for methane and carbon dioxide activation. Equally important thing is selecting the proper support materials having labile oxygen (CeO_2, TiO_2, or $SrTiO_3$), to maximize the H_2:CO ratio and lifetime of catalyst by preventing carbon deposition.

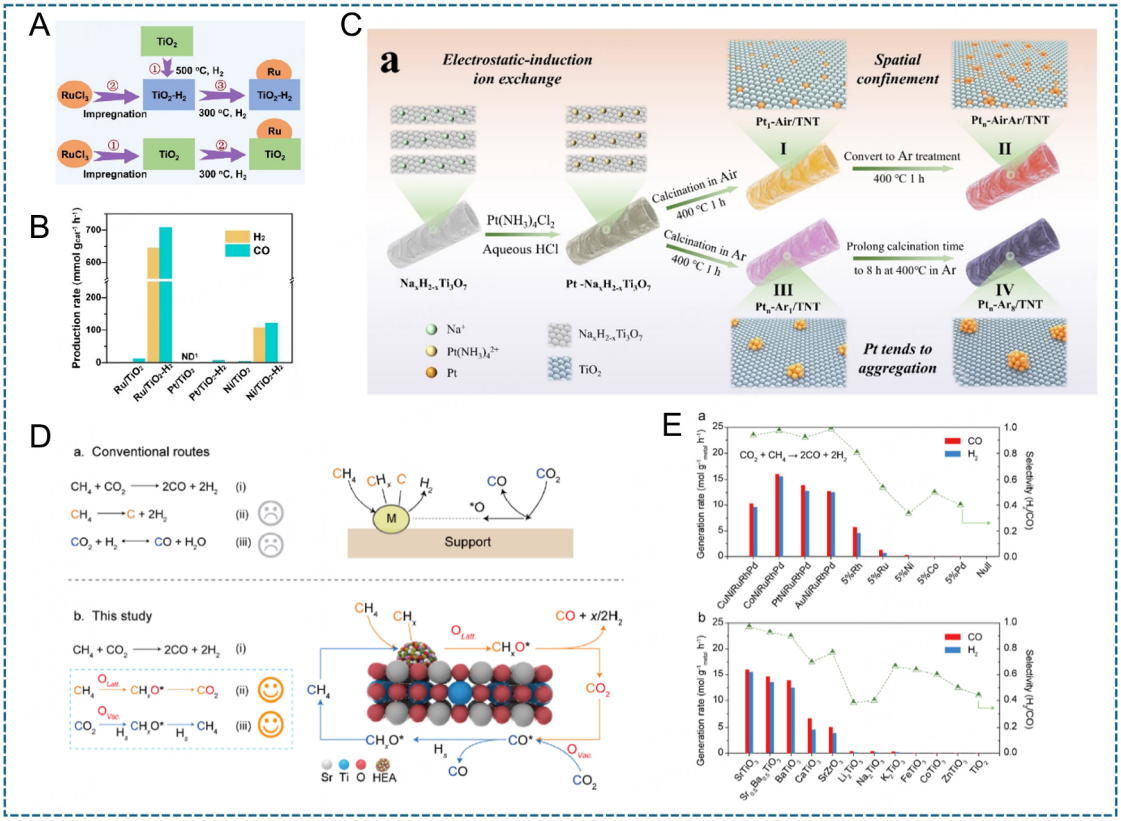

Figure 16. Dry reforming of methane reaction catalyzed by platinum group metal (PGM)-based photothermal catalytic materials: (A) Illustration of the synthesis process of Ru/TiO_2-H_2 and Ru/TiO_2. (B) Average production rates of H_2 and CO over Ru, Pt, and Ni/TiO_2 with controlled SMSI under focused full-spectrum light irradiation. Reproduced with permission from Ref.[88] (C) Schematic illustration of the synthesis process for TNT and Pt/TNT samples. Reproduced with permission from Ref.[92] (D) Schematic illustration of the proposed processes of DRM, which involves the carbon exchange between reactants and the oxygen exchange between CO_2 and the lattice oxygen of supports. (E) Light-driven DRM yields of H_2 and CO by mono- and quinary-component metal-loaded $SrTiO_3$ catalysts and HEA-loaded catalysts. Reproduced with permission from Ref.[86].

Nonthermal effect of light on H_2/CO ratio

Many researchers report the results of photothermal DRM reactions using various catalytic materials as previously mentioned, but it is difficult to directly compare the reaction rates since each reaction system and method of light irradiation is different. However, one common phenomenon is that the H_2:CO ratio is observed to be much higher when light energy is present compared to dark experiments. This implies that light energy not only simply increases the reaction rate but also plays a significant role in increasing the H_2 yield. In 2022, Takami *et al.* investigated the photothermal DRM over Rh NPs supported on Al_2O_3 using a combination of Vis and NIR light irradiation, with the primary objective being to understand how photoinduced heating at the nanoscale during DRM affects the catalytic activity and local temperature of Rh NPs [Figure 17A][90]. The researchers used operational dispersive X-ray absorption spectroscopy (DXAS) to capture the real-time changes in temperature and chemical state of the Rh particles. The DXAS technique can directly measure the local temperature of Rh NPs exposed to light, enabling them to precisely track the transient heating effect and its impact on the reaction. To elaborate in more detail, Debye-Waller factor (σ) is utilized for temperature determination from DXAS. Debye-Waller factor is a parameter that describes the effects of structural and vibrational disorder on extended X-ray absorption fine structure (EXAFS) signals. This factor is related to the mean-square fluctuations in interatomic distances, and is also known as the B factor, which expresses the magnitude of thermal vibrations of atoms. As the magnitude of thermal vibrations of atoms increases with temperature, the calculated Debye-Waller factor from EXAFS signal also

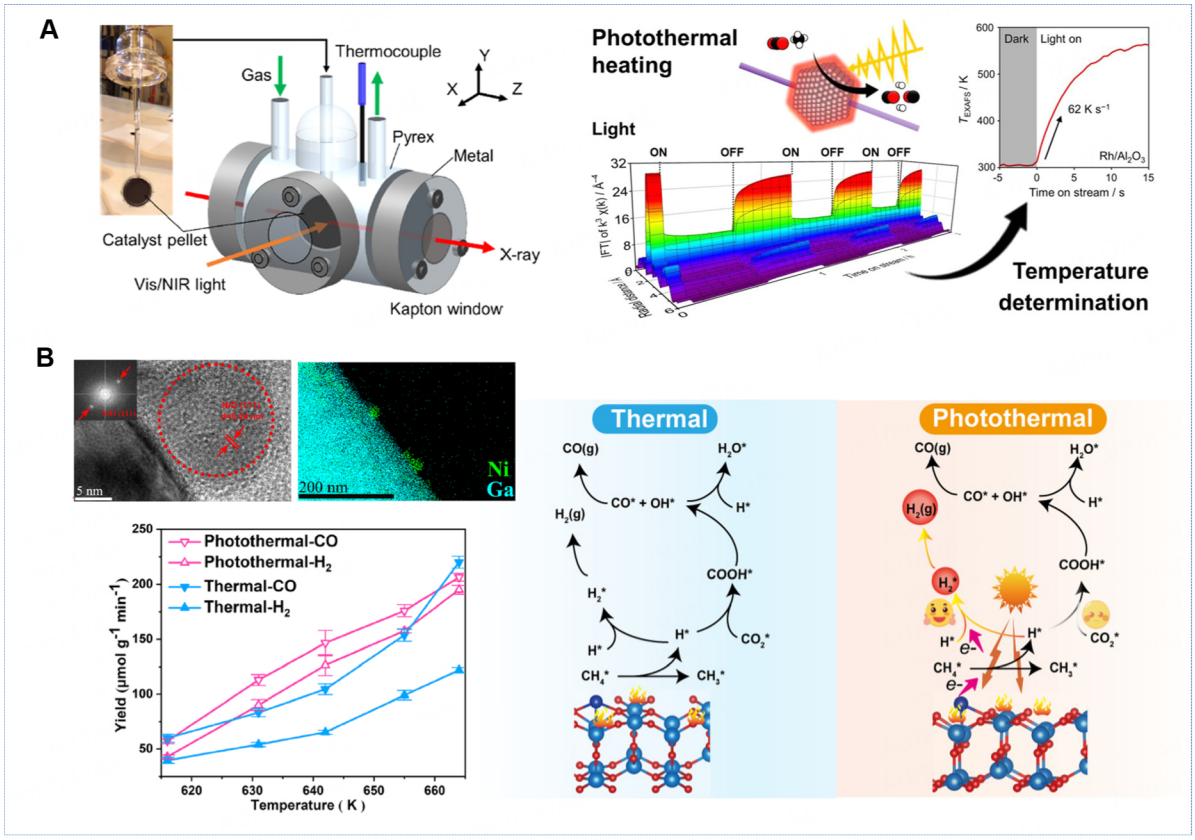

Figure 17. (A) Schematic diagram of the photothermal reactor used in operando DXAS under concentrated visible and near-infrared light to evaluate the temperature of the catalytic active sites of Rh NPs on Al_2O_3. Reproduced with permission from Ref.[90]. (B) HRTEM image and EDS mapping of the Ni/Ga_2O_3 catalyst. DRM catalytic performances over Ni/Ga_2O_3 catalyst at different temperatures. Schematic diagram of the photothermal catalytic mechanism of the Ni/Ga_2O_3 catalyst. Reproduced with permission from Ref.[89].

increases. Fortunately, it has been experimentally demonstrated that the square of the Debye-Waller factor (σ^2) and temperature are well fitted by linear function. This is why the Debye-Waller factor can be used as indicators to estimate the temperature of local environment of metal NPs. Interestingly, the local temperature of Rh NPs measured by operando DXAS reached values significantly higher than the bulk reactor temperature. The local temperature of Rh NPs measured by the light source was up to 630 K, while the bulk reactor temperature measured by the thermocouple was significantly lower, approximately 473 K. This discrepancy between the local and bulk temperatures demonstrates how light directly heats Rh NPs, creating local hot spots that drive the dry reforming reaction more efficiently even at relatively low bulk reactor temperatures. Overall, this local heating effect is directly related to the high CH_4 and CO_2 conversions achieved under photothermal conditions. In addition, they found that smaller Rh NPs exhibited faster temperature responses and higher catalytic activity, suggesting that NP size and local heat generation have correlated with each other and are important for optimizing DRM performance. Another observation was that the H_2 fraction under photoirradiation was consistently higher than that of conventional thermal DRM reactions, showing a presence of strong nonthermal effect of light on the product selectivity. In 2021, Rao *et al.* investigated the role of nonthermal photoeffects in the photothermal DRM over Ni/Ga_2O_3 catalysts is investigated [Figure 17B][89]. The researchers performed both photothermal and thermal catalytic tests in the temperature range of 616-664 K to explore how light irradiation affects the H_2/CO ratio during DRM. The catalysts were synthesized using a wet impregnation method with 5 wt% Ni loading. They measured the formation rates of H_2 and CO, and performed *in situ* DRIFTS to investigate the

species adsorbed on the catalyst surface under light irradiation. They suggested reasonable explanation on how the light irradiation can promote H_2 formation by distinct nonthermal effects that alter the surface reaction. The suppression of RWGS allows more hydrogen to form, thus increasing the H_2/CO ratio. To summarize, the work demonstrates that light irradiation not only heats the catalyst but also introduces nonthermal effects that significantly enhance H_2 production and alter the reaction pathways in DRM, achieving a more favorable product distribution.

CONCLUSION AND OUTLOOK

In summary, the current understanding of the photothermal catalytic mechanisms was described on how light irradiation can affect catalytic reactions including plasmonic light absorption, hot carrier generation, photon to phonon conversion and local heating effect. The initial step in photothermal processes is the design of plasmonic light absorbers that can efficiently harness light. Therefore, the development of plasmonic photothermal catalysts requires a strategic focus on material selection, structural optimization, and scalable synthesis. Combining plasmonic metals with dielectric materials can enhance charge separation and heat retention. Simultaneously, tailoring NP size, shape, and hybrid structures allows precise control over light absorption and catalytic activity. Scalable synthesis methods, such as hydrothermal growth and galvanic replacement, offer practical pathways for large-scale applications.

Previous studies on photocatalysts have often overlooked the role of localized heat effects, focusing instead on light absorption, charge carriers, and catalytic performance. To develop more effective photothermal catalysts, it is crucial to distinguish and analyze the separate contributions of photocatalysis from charge carriers and thermal effects from local heating. However, monitoring nanoscale surface temperatures remains challenging due to limitations in conventional measurement techniques. Advancing non-intrusive methods and accurate computational models to estimate local temperature gradients will be key to optimizing the synergistic effects of these phenomena.

Recent photothermal catalysts are categorically summarized by focusing on CO_2 hydrogenation and DRM reactions. The works on CO_2 hydrogenation demonstrate significant progress and offer directions for developing efficient catalysts. One of the challenges to be addressed is the development of economically viable catalysts. In CO_2 methanation reactions, there is a tendency to use Ru extensively. To overcome this, research has been conducted using Ni, but issues such as coking and sintering remain unresolved. The problems observed in thermal catalysis persist in the field of photothermal catalysis as well. In the RWGS reaction, considerable research has been done on catalyst structure design, which helps understand the photothermal effect and the impact of structural changes on reactivity. However, the challenge is the limited research on the use of real solar energy for photothermal catalysts. Therefore, future studies require additional discussion on how to efficiently utilize the actual solar energy in practical catalytic systems. In methanol production, the reaction tends to show a much slower reaction rate and lower yield compared to other processes, and there is still a lack of information on the mechanistic details. Additionally, the use of high-intensity light sources poses a limitation for commercial applications. As the understanding of mechanisms and photothermal effects for RWGS and CO_2 methanation reactions has improved, future research should focus on practical applications.

Catalyst stability during prolonged reactions is also a major challenge in photothermal catalysis. Long-term exposure to high temperatures, reactive intermediates, and frequent thermal cycling can lead to deactivation through coking, sintering, and poisoning. To address these issues, future research should focus on strategies such as alloying, surface modification, and the incorporation of robust support materials to improve catalyst resistance. Also, focusing on understanding catalyst deactivation mechanisms is essential for addressing

long-term operational challenges. Potential solutions include designing catalysts with self-regenerating properties, optimizing reaction conditions to prevent coke formation, and employing in situ regeneration to restore activity during operation. Scalability of photothermal systems presents another critical challenge because Lab-scale experiments often use high-intensity light sources such as lasers or concentrated solar setups, which are not feasible for industrial applications. Efficient reactor designs, uniform light distribution, and innovative optical materials will be needed to transition photothermal systems from research to industrial scales. In addition, emerging approaches such as machine learning (ML) for catalyst optimization are poised to revolutionize the design of photothermal catalysis. Nowadays, ML can analyze vast experimental and computational datasets to predict catalyst performance and accelerate the discovery of new materials. Similarly, advanced in situ techniques, such as operando spectroscopy, X-ray absorption, and ultrafast microscopy, provide insights into photothermal effects at the molecular level. These enable real-time monitoring of photothermal catalyst structure and reaction intermediates on the surface. These tools are indispensable for elucidating reaction mechanisms and tuning catalyst properties.

Lastly, tandem catalyst design is expected to be a promising approach to improve the efficiency of photothermal catalytic processes. Combining different catalysts that work optimally at different reaction stages can facilitate sequential reactions, thereby improving the overall process yield and selectivity. This strategy can effectively address the limitations associated with single-purpose catalysts, normally with narrow operating windows and limited activity. For example, integrating a photothermal catalyst that produces hydrogen in a photothermal water-splitting reaction with a subsequent catalyst for CO_2 reduction can significantly enhance the production of valuable fuels and chemicals. Likewise, developing a tandem catalytic system that integrates the syngas production and Fisher-Tropsch reaction for hydrocarbon fuel production can minimize the total energy required for storage and transportation of syngas. In this way, tandem systems can maximize the synergy between photothermal reactions by reducing energy consumption and increasing process yield since the output of one reaction step becomes the input for the next catalytic reaction. Thus, future research should focus on optimizing the interaction between different photothermal catalysts in a tandem catalytic system and exploring how different types of light energy can affect each catalytic performance. Such an approach may pave the way for more sustainable and efficient catalytic processes, ultimately contributing to realizing commercial applications of photothermal catalysis.

DECLARATIONS

Authors' contributions

Conceptualization and funding acquisition, writing-review & editing, and supervision, guidance for the review, including language checking and polishing: Song, I.; Dong, W.
Investigation, visualization, and writing-original draft: Choi, S. H.; Song, I.; Dong, W. J.

Availability of data and materials

Not applicable.

Financial support and sponsorship

This work was supported by the Korea Institute of Energy Technology Evaluation and Planning (KETEP) and granted financial resources from the Ministry of Trade, Industry & Energy, Republic of Korea, 20213091010020; National Research Foundation of Korea (NRF) grant funded by the Korea government (MSIT), RS-2024-00455924.

Conflicts of interest

All authors declared that there are no conflicts of interest.

Ethical approval and consent to participate

Not applicable.

Consent for publication

Not applicable.

Copyright

REFERENCES

1. Sullivan, I.; Goryachev, A.; Digdaya, I. A.; et al. Author correction: coupling electrochemical CO_2 conversion with CO_2 capture. *Nat. Catal.* **2022**, *5*, 75-6. DOI
2. Dong, W. J.; Mi, Z. One-dimensional III-nitrides: towards ultrahigh efficiency, ultrahigh stability artificial photosynthesis. *J. Mater. Chem. A.* **2023**, *11*, 5427-59. DOI
3. Bushuyev, O. S.; De Luna, P.; Dinh, C. T.; et al. What should we make with CO_2 and how can we make it? *Joule* **2018**, *2*, 825-32. DOI
4. Zhang, F.; Li, Y.; Qi, M.; et al. Photothermal catalytic CO_2 reduction over nanomaterials. *Chem. Catal.* **2021**, *1*, 272-97. DOI
5. Liu, H.; Gao, X.; Shi, D.; et al. Recent progress on photothermal heterogeneous catalysts for CO_2 conversion reactions. *Energy. Technol.* **2022**, *10*, 2100804. DOI
6. Fan, W. K.; Tahir, M. Recent developments in photothermal reactors with understanding on the role of light/heat for CO_2 hydrogenation to fuels: a review. *Chem. Eng. J.* **2022**, *427*, 131617. DOI
7. Luo, S.; Ren, X.; Lin, H.; Song, H.; Ye, J. Plasmonic photothermal catalysis for solar-to-fuel conversion: current status and prospects. *Chem. Sci.* **2021**, *12*, 5701-19. DOI PubMed PMC
8. Lv, C.; Bai, X.; Ning, S.; et al. Nanostructured materials for photothermal carbon dioxide hydrogenation: regulating solar utilization and catalytic performance. *ACS. Nano.* **2023**, *17*, 1725-38. DOI
9. Cai, M.; Li, C.; An, X.; et al. Supra-photothermal CO_2 methanation over greenhouse-like plasmonic superstructures of ultrasmall cobalt nanoparticles. *Adv. Mater.* **2024**, *36*, e2308859. DOI
10. Meng, X.; Wang, T.; Liu, L.; et al. Photothermal conversion of CO_2 into CH_4 with H_2 over group VIII nanocatalysts: an alternative approach for solar fuel production. *Angew. Chem. Int. Ed.* **2014**, *53*, 11478-82. DOI
11. Ren, J.; Ouyang, S.; Xu, H.; et al. Targeting activation of CO_2 and H_2 over Ru-loaded ultrathin layered double hydroxides to achieve efficient photothermal CO_2 methanation in flow-type system. *Adv. Energy. Mater.* **2017**, *7*, 1601657. DOI
12. Mateo, D.; Albero, J.; García, H. Graphene supported NiO/Ni nanoparticles as efficient photocatalyst for gas phase CO_2 reduction with hydrogen. *Appl. Catal. B. Environ.* **2018**, *224*, 563-71. DOI
13. Ali, F. M.; Ghuman, K. K.; O'brien, P. G.; et al. Highly efficient ambient temperature CO_2 photomethanation catalyzed by nanostructured RuO_2 on silicon photonic crystal support. *Adv. Energy. Mater.* **2018**, *8*, 1702277. DOI
14. Mateo, D.; Albero, J.; García, H. Titanium-perovskite-supported RuO_2 nanoparticles for photocatalytic CO_2 methanation. *Joule* **2019**, *3*, 1949-62. DOI
15. Li, Y.; Hao, J.; Song, H.; et al. Selective light absorber-assisted single nickel atom catalysts for ambient sunlight-driven CO_2 methanation. *Nat. Commun.* **2019**, *10*, 2359. DOI PubMed PMC
16. Mateo, D.; Morlanes, N.; Maity, P.; Shterk, G.; Mohammed, O. F.; Gascon, J. Efficient visible-light driven photothermal conversion of CO_2 to methane by nickel nanoparticles supported on barium titanate. *Adv. Funct. Mater.* **2021**, *31*, 2008244. DOI
17. Fu, G.; Jiang, M.; Liu, J.; et al. Rh/Al nanoantenna photothermal catalyst for wide-spectrum solar-driven CO_2 methanation with nearly 100% selectivity. *Nano. Lett.* **2021**, *21*, 8824-30. DOI
18. Zhou, L.; Martirez, J. M. P.; Finzel, J.; et al. Light-driven methane dry reforming with single atomic site antenna-reactor plasmonic photocatalysts. *Nat. Energy.* **2020**, *5*, 61-70. DOI
19. Tang, Y.; Li, Y.; Bao, W.; et al. Enhanced dry reforming of CO_2 and CH_4 on photothermal catalyst Ru/$SrTiO_3$. *Appl. Catal. B. Environ.* **2023**, *338*, 123054. DOI
20. Huang, H.; Mao, M.; Zhang, Q.; et al. Solar-light-driven CO_2 reduction by CH_4 on silica-cluster-modified Ni nanocrystals with a high solar-to-fuel efficiency and excellent durability. *Adv. Energy. Mater.* **2018**, *8*, 1702472. DOI
21. Zhang, J.; Xie, K.; Jiang, Y.; et al. Photoinducing different mechanisms on a Co-Ni bimetallic alloy in catalytic dry reforming of methane. *ACS. Catal.* **2023**, *13*, 10855-65. DOI
22. Shoji, S.; Peng, X.; Yamaguchi, A.; et al. Photocatalytic uphill conversion of natural gas beyond the limitation of thermal reaction systems. *Nat. Catal.* **2020**, *3*, 148-53. DOI
23. Li, Y.; Liu, X.; Wu, T.; et al. Pulsed laser induced plasma and thermal effects on molybdenum carbide for dry reforming of methane. *Nat. Commun.* **2024**, *15*, 5495. DOI PubMed PMC
24. Li, Y.; Li, D.; Liu, H.; et al. *In situ* fabricating a Rh/Ga_2O_3 photothermal catalyst for dry reforming of methane. *Catal. Sci. Technol.* **2024**, *14*, 2722-9. DOI

25. Ulmer, U.; Dingle, T.; Duchesne, P. N.; et al. Fundamentals and applications of photocatalytic CO_2 methanation. *Nat. Commun.* **2019**, *10*, 3169. DOI PubMed PMC
26. Feng, K.; Wang, S.; Zhang, D.; et al. Cobalt plasmonic superstructures enable almost 100% broadband photon efficient CO_2 photocatalysis. *Adv. Mater.* **2020**, *32*, e2000014. DOI
27. Dong, W. J.; Yu, H. K.; Lee, J. L. Abnormal dewetting of Ag layer on three-dimensional ITO branches to form spatial plasmonic nanoparticles for organic solar cells. *Sci. Rep.* **2020**, *10*, 12819. DOI PubMed PMC
28. Cho, W. S.; Park, J. Y.; Yu, H. K.; Dong, W. J.; Lee, J. Simple and reversible method to control the surface energy of ITO branched nanowires for tuning wettability of micro/nanoscale droplets. *App. Surf. Sci.* **2025**, *679*, 161227. DOI
29. Zhang, J. Z.; Noguez, C. Plasmonic optical properties and applications of metal nanostructures. *Plasmonics* **2008**, *3*, 127-50. DOI
30. Clavero, C. Plasmon-induced hot-electron generation at nanoparticle/metal-oxide interfaces for photovoltaic and photocatalytic devices. *Nat. Photon.* **2014**, *8*, 95-103. DOI
31. Brongersma, M. L.; Halas, N. J.; Nordlander, P. Plasmon-induced hot carrier science and technology. *Nat. Nanotechnol.* **2015**, *10*, 25-34. DOI PubMed
32. Zhang, X.; Chen, Y. L.; Liu, R. S.; Tsai, D. P. Plasmonic photocatalysis. *Rep. Prog. Phys.* **2013**, *76*, 046401. DOI
33. Kumar, A.; Choudhary, P.; Kumar, A.; Camargo, P. H. C.; Krishnan, V. Recent advances in plasmonic photocatalysis based on TiO_2 and noble metal nanoparticles for energy conversion, environmental remediation, and organic synthesis. *Small* **2022**, *18*, e2101638. DOI
34. DuChene, J. S.; Tagliabue, G.; Welch, A. J.; Cheng, W. H.; Atwater, H. A. Hot hole collection and photoelectrochemical CO_2 reduction with plasmonic Au/p-GaN photocathodes. *Nano. Lett.* **2018**, *18*, 2545-50. DOI PubMed
35. Jiang, X.; Huang, J.; Bi, Z.; et al. Plasmonic active "hot spots"-confined photocatalytic CO_2 reduction with high selectivity for CH_4 production. *Adv. Mater.* **2022**, *34*, e2109330. DOI
36. Baffou, G.; Quidant, R. Thermo-plasmonics: using metallic nanostructures as nano-sources of heat. *Laser. Photonics. Rev.* **2013**, *7*, 171-87. DOI
37. Chen, J.; Ye, Z.; Yang, F.; Yin, Y. Plasmonic nanostructures for photothermal conversion. *Small. Sci.* **2021**, *1*, 2000055. DOI
38. Linic, S.; Aslam, U.; Boerigter, C.; Morabito, M. Photochemical transformations on plasmonic metal nanoparticles. *Nat. Mater.* **2015**, *14*, 567-76. DOI
39. Jiang, W.; Low, B. Q. L.; Long, R.; et al. Active site engineering on plasmonic nanostructures for efficient photocatalysis. *ACS. Nano.* **2023**, *17*, 4193-229. DOI
40. Cai, M.; Wu, Z.; Li, Z.; et al. Greenhouse-inspired supra-photothermal CO_2 catalysis. *Nat. Energy.* **2021**, *6*, 807-14. DOI
41. Coppens, Z. J.; Li, W.; Walker, D. G.; Valentine, J. G. Probing and controlling photothermal heat generation in plasmonic nanostructures. *Nano. Lett.* **2013**, *13*, 1023-8. DOI PubMed
42. Mateo, D.; Cerrillo, J. L.; Durini, S.; Gascon, J. Fundamentals and applications of photo-thermal catalysis. *Chem. Soc. Rev.* **2021**, *50*, 2173-210. DOI
43. Sun, C.; Zhao, Z.; Liu, H.; Wang, H. Core-shell nanostructure for supra-photothermal CO_2 catalysis. *Rare. Met.* **2022**, *41*, 1403-5. DOI
44. Chen, X.; Chen, Y.; Yan, M.; Qiu, M. Nanosecond photothermal effects in plasmonic nanostructures. *ACS. Nano.* **2012**, *6*, 2550-7. DOI
45. Xiong, Y.; Zhao, W.; Gu, D.; Tie, Z.; Zhang, W.; Jin, Z. Tunable C_2 products via photothermal steam reforming of CO_2 over surface-modulated mesoporous cobalt oxides. *Nano. Lett.* **2023**, *23*, 4876-84. DOI
46. Tang, X.; Song, C.; Li, H.; et al. Thermally stable Ni foam-supported inverse $CeAlO_x$/Ni ensemble as an active structured catalyst for CO_2 hydrogenation to methane. *Nat. Commun.* **2024**, *15*, 3115. DOI PubMed PMC
47. Li, N.; Liu, M.; Yang, B.; et al. Enhanced photocatalytic performance toward CO_2 hydrogenation over nanosized TiO_2-loaded Pd under UV irradiation. *J. Phys. Chem. C.* **2017**, *121*, 2923-32. DOI
48. Deng, B.; Song, H.; Peng, K.; Li, Q.; Ye, J. Metal-organic framework-derived Ga-Cu/CeO_2 catalyst for highly efficient photothermal catalytic CO_2 reduction. *Appl. Catal. B. Environ.* **2021**, *298*, 120519. DOI
49. Tang, Y.; Wang, H.; Guo, C.; et al. Ruthenium-cobalt solid-solution alloy nanoparticles for enhanced photopromoted thermocatalytic CO_2 hydrogenation to methane. *ACS. Nano.* **2024**, *18*, 11449-61. DOI
50. Peng, K.; Ye, J.; Wang, H.; et al. Natural halloysite nanotubes supported Ru as highly active catalyst for photothermal catalytic CO_2 reduction. *Appl. Catal. B. Environ.* **2023**, *324*, 122262. DOI
51. Ge, H.; Kuwahara, Y.; Kusu, K.; Bian, Z.; Yamashita, H. Ru/H MoO_3- with plasmonic effect for boosting photothermal catalytic CO_2 methanation. *Appl. Catal. B. Environ.* **2022**, *317*, 121734. DOI
52. Du, P.; Deng, G.; Li, Z.; et al. Effective CO_2 activation of enriched oxygen vacancies for photothermal CO_2 methanation. *J. Mater. Sci. Technol.* **2024**, *189*, 203-10. DOI
53. Zhai, J.; Xia, Z.; Zhou, B.; et al. Photo-thermal coupling to enhance CO_2 hydrogenation toward CH_4 over Ru/MnO/Mn_3O_4. *Nat. Commun.* **2024**, *15*, 1109. DOI PubMed PMC
54. Guo, C.; Tang, Y.; Yang, Z.; et al. Reinforcing the efficiency of photothermal catalytic CO_2 methanation through integration of Ru nanoparticles with photothermal $MnCo_2O_4$ nanosheets. *ACS. Nano.* **2023**, *17*, 23761-71. DOI
55. Zhu, X.; Zong, H.; Pérez, C. J. V.; et al. Supercharged CO_2 photothermal catalytic methanation: high conversion, rate, and selectivity. *Angew. Chem. Int. Ed.* **2023**, *135*, e202218694. DOI

56. Li, Q.; Wang, C.; Wang, H.; Chen, J.; Chen, J.; Jia, H. Disclosing support-size-dependent effect on ambient light-driven photothermal CO_2 hydrogenation over nickel/titanium dioxide. *Angew. Chem. Int. Ed.* **2024**, *136*, e202318166. DOI
57. Vrijburg, W. L.; Moioli, E.; Chen, W.; et al. Efficient base-metal NiMn/TiO_2 catalyst for CO_2 methanation. *ACS. Catal.* **2019**, *9*, 7823-39. DOI
58. Guo, J.; Duchesne, P. N.; Wang, L.; et al. High-performance, scalable, and low-cost copper hydroxyapatite for photothermal CO_2 reduction. *ACS. Catal.* **2020**, *10*, 13668-81. DOI
59. Zhao, J.; Yang, Q.; Shi, R.; et al. FeO-CeO_2 nanocomposites: an efficient and highly selective catalyst system for photothermal CO_2 reduction to CO. *NPG. Asia. Mater.* **2020**, *12*, 171. DOI
60. Lou, D.; Xu, A.; Fang, Y.; et al. Cobalt-sputtered anodic aluminum oxide membrane for efficient photothermal CO_2 hydrogenation. *ChemNanoMat* **2021**, *7*, 1008-12. DOI
61. Zhao, Z.; Doronkin, D. E.; Ye, Y.; Grunwaldt, J.; Huang, Z.; Zhou, Y. Visible light-enhanced photothermal CO_2 hydrogenation over Pt/Al_2O_3 catalyst. *Chin. J. Catal.* **2020**, *41*, 286-93. DOI
62. Tang, Y.; Wu, S.; Wang, Y.; et al. Photo-Assisted Catalytic CO_2 hydrogenation to CO with nearly 100% selectivity over Rh/TiO_2 catalysts. *Energy. Fuels.* **2023**, *37*, 539-46. DOI
63. Yang, Z.; Zhao, T.; Tang, Y.; et al. Size-modulated photo-thermal catalytic CO_2 hydrogenation performances over Pd nanoparticles. *J. Catal.* **2023**, *424*, 22-8. DOI
64. Su, X.; Yang, X.; Zhao, B.; Huang, Y. Designing of highly selective and high-temperature endurable RWGS heterogeneous catalysts: recent advances and the future directions. *J. Energy. Chem.* **2017**, *26*, 854-67. DOI
65. Lu, B.; Quan, F.; Sun, Z.; Jia, F.; Zhang, L. Photothermal reverse-water-gas-shift over Au/CeO_2 with high yield and selectivity in CO_2 conversion. *Catal. Commun.* **2019**, *129*, 105724. DOI
66. Wang, L.; Dong, Y.; Yan, T.; et al. Black indium oxide a photothermal CO_2 hydrogenation catalyst. *Nat. Commun.* **2020**, *11*, 2432. DOI PubMed PMC
67. Peng, Y.; Szalad, H.; Nikacevic, P.; et al. Co-doped hydroxyapatite as photothermal catalyst for selective CO_2 hydrogenation. *Appl. Catal. B. Environ.* **2023**, *333*, 122790. DOI
68. Wang, J.; Li, S.; Zhao, J.; Liu, K.; Jiang, B.; Li, H. Boron-doped Cu-Co catalyst boosting charge transfer in photothermal carbon dioxide hydrogenation. *Appl. Catal. B. Environ. Energy.* **2024**, *352*, 124045. DOI
69. Tan, W.; Xie, S.; Zhang, X.; et al. Fine-tuning of Pt dispersion on Al_2O_3 and understanding the nature of active Pt sites for efficient CO and NH_3 oxidation reactions. *ACS. Appl. Mater. Interfaces.* **2024**, *16*, 454-66. DOI
70. Kiss, A. A.; Pragt, J.; Vos, H.; Bargeman, G.; de, G. M. Novel efficient process for methanol synthesis by CO_2 hydrogenation. *Chem. Eng. J.* **2016**, *284*, 260-9. DOI
71. Barberis, L.; Hakimioun, A. H.; Plessow, P. N.; et al. Competition between reverse water gas shift reaction and methanol synthesis from CO_2: influence of copper particle size. *Nanoscale* **2022**, *14*, 13551-60. DOI
72. Wang, Z.; Song, H.; Pang, H.; et al. Photo-assisted methanol synthesis via CO_2 reduction under ambient pressure over plasmonic Cu/ZnO catalysts. *Appl. Catal. B. Environ.* **2019**, *250*, 10-6. DOI
73. Deng, B.; Song, H.; Wang, Q.; et al. Highly efficient and stable photothermal catalytic CO_2 hydrogenation to methanol over Ru/In_2O_3 under atmospheric pressure. *Appl. Catal. B. Environ.* **2023**, *327*, 122471. DOI
74. Xie, B.; Wong, R. J.; Tan, T. H.; et al. Synergistic ultraviolet and visible light photo-activation enables intensified low-temperature methanol synthesis over copper/zinc oxide/alumina. *Nat. Commun.* **2020**, *11*, 1615. DOI PubMed PMC
75. Wu, D.; Deng, K.; Hu, B.; Lu, Q.; Liu, G.; Hong, X. Plasmon-assisted photothermal catalysis of low-pressure CO_2 hydrogenation to methanol over Pd/ZnO catalyst. *ChemCatChem* **2019**, *11*, 1598-601. DOI
76. Zhang, G.; Xu, Q.; Huang, H.; et al. Ni-doped In_2O_3 photothermal coupling catalyzed boosted carbon dioxide hydrogenation to methanol. *Ind. Eng. Chem. Res.* **2024**, *63*, 968-79. DOI
77. Wang, L.; Ghoussoub, M.; Wang, H.; et al. Photocatalytic hydrogenation of carbon dioxide with high selectivity to methanol at atmospheric pressure. *Joule* **2018**, *2*, 1369-81. DOI
78. Zhang, Z.; Mao, C.; Meira, D. M.; et al. New black indium oxide - tandem photothermal CO_2-H_2 methanol selective catalyst. *Nat. Commun.* **2022**, *13*, 1512. DOI PubMed PMC
79. Xie, T.; Zhang, Z.; Zheng, H.; Xu, K.; Hu, Z.; Lei, Y. Enhanced photothermal catalytic performance of dry reforming of methane over Ni/mesoporous TiO_2 composite catalyst. *Chem. Eng. J.* **2022**, *429*, 132507. DOI
80. Han, K.; Wang, Y.; Wang, S.; Liu, Q.; Deng, Z.; Wang, F. Narrowing band gap energy of CeO_2 in (Ni/CeO_2)@SiO_2 catalyst for photothermal methane dry reforming. *Chem. Eng. J.* **2021**, *421*, 129989. DOI
81. Takami, D.; Tsubakimoto, J.; Sarwana, W.; Yamamoto, A.; Yoshida, H. Photothermal dry reforming of methane over phyllosilicate-derived silica-supported nickel catalysts. *ACS. Appl. Energy. Mater.* **2023**, *6*, 7627-35. DOI
82. Hu, B.; Wang, B.; Zhou, W.; et al. Synergistic effect of Ru single atom and nanoparticle on photothermal methane dry reforming reaction. *Chem. Eng. Sci.* **2024**, *297*, 120308. DOI
83. Yang, Y.; Chai, Z.; Qin, X.; et al. Light-induced redox looping of a rhodium/Ce_xWO_3 photocatalyst for highly active and robust dry reforming of methane. *Angew. Chem. Int. Ed.* **2022**, *61*, e202200567. DOI
84. Liu, H.; Song, H.; Zhou, W.; Meng, X.; Ye, J. A promising application of optical hexagonal TaN in photocatalytic reactions. *Angew. Chem. Int. Ed.* **2018**, *130*, 17023-6. DOI
85. Rao, Z.; Wang, K.; Cao, Y.; et al. Light-reinforced key intermediate for anticoking to boost highly durable methane dry reforming over

single atom Ni active sites on CeO_2. *J. Am. Chem. Soc.* **2023**, *145*, 24625-35. DOI

86. Xiong, H.; Dong, Y.; Hu, C.; et al. Highly efficient and selective light-driven dry reforming of methane by a carbon exchange mechanism. *J. Am. Chem. Soc.* **2024**, *146*, 9465-75. DOI
87. Tavasoli, A.; Gouda, A.; Zähringer, T.; et al. Enhanced hybrid photocatalytic dry reforming using a phosphated Ni-CeO_2 nanorod heterostructure. *Nat. Commun.* **2023**, *14*, 1435. DOI PubMed PMC
88. Li, Q.; Wang, H.; Zhang, M.; Li, G.; Chen, J.; Jia, H. Suppressive strong metal-support interactions on ruthenium/TiO_2 promote light-driven photothermal CO_2 reduction with methane. *Angew. Chem. Int. Ed.* **2023**, *135*, e202300129. DOI
89. Rao, Z.; Cao, Y.; Huang, Z.; et al. Insights into the nonthermal effects of light in dry reforming of methane to enhance the H_2/CO ratio near unity over Ni/Ga_2O_3. *ACS. Catal.* **2021**, *11*, 4730-8. DOI
90. Takami, D.; Yamamoto, A.; Kato, K.; Shishido, T.; Yoshida, H. Transient temperature response of supported Rh nanoparticles in photothermal dry reforming of methane - an *Operando* dispersive X-ray absorption spectroscopy study. *J. Phys. Chem. C.* **2022**, *126*, 15736-43. DOI
91. Zhang, J.; Li, Y.; Sun, J.; et al. Regulation of energetic hot carriers on Pt/TiO_2 with thermal energy for photothermal catalysis. *Appl. Catal. B. Environ.* **2022**, *309*, 121263. DOI
92. He, C.; Li, Q.; Ye, Z.; et al. Regulating atomically-precise Pt sites for boosting light-driven dry reforming of methane. *Angew. Chem. Int. Ed.* **2024**, *63*, e202412308. DOI